공학박사 학위논문

Quantification of the plasma treatment on biotargets via ROS measurement in terms of equivalent radiation dose

활성산소종 측정을 통한 등가방사선량 개념의 플라즈마 처치 정량화 연구

2020 년 2 월

서울대학교 대학원

에너지시스템공학부

지 완 욱

활성산소종 측정을 통한 등가방사선량 개념의 플라즈마 처치 정량화 연구

지도 교수 김 은 희

이 논문을 공학박사 학위논문으로 제출함
2020년 2월

서울대학교 대학원
에너지시스템공학부
지 완 욱

지완욱의 공학박사 학위논문을 인준함
2020년 2월

위 원 장 김 곤 호 (인)

부위원장 김 은 희 (인)

위 원 정 경 재 (인)

위 원 조 영 환 (인)

위 원 배 상 우 (인)

ABSTRACT

Quantification of plasma treatment on biotargets via ROS measurement in terms of equivalent radiation dose

Ji, Wanook

Department of Energy Systems Engineering
The Graduate School
Seoul National University

Non-thermal plasma has been studied for medical purposes such as sterilization, bacterial deactivation, wound healing, and cancer treatment. One of the problem is that the concept of plasma dosimetry has not been defined yet. Most of laboratories set up the operational parameters usually treatment time to control the dose based on empirical data. In this study, we suggest the concept of quantification of plasma dose by comparing with radiation dose.

Non-thermal plasma generates physical factors including electromagnetic fields, heat and UV and also chemical factors including reactive oxygen and nitrogen species (RONS). Several studies reported ROS, especially hydroxyl radical (OH radical), play main roles in the plasma medicine. Low linear energy transfer (LET) radiation mostly induces cell death by producing OH radical via water radiolysis. Considering that both non-thermal plasmas and radiations produce OH radical as main

mediator, plasma treatment could be quantified by comparing OH radical production with equivalent radiation dose. In this study, atmospheric pressure plasma jet (APPJ) reactor was used to generate non-thermal plasma and hard X-ray beam facility was used to generate X-ray. To measure OH radical generated in medium which has very short half-life, spin trapping material was used to measure by ESR spectrometry. DMPO-OH adduct has relatively long half-life (870s).

Low LET radiation (X-ray) and plasma has difference for producing OH radicals. In contrast, X-ray produced OH radicals homogeneously with penetrating effect, APPJ produced most of OH radicals at medium surface without penetrating effect. Measuring intracellular OH radical was conducted to assess OH production inside the cells. The clonogenic surviving fraction (SF) assay was conducted to assess cell proliferation ability after treatment. The equivalent radiation doses were derived from comparing DMPO-OH concentration, intracellular OH concentration, and clonogenic SF of plasma treatments.

We could conclude that the correlation between intracellular ROS and clonogenic SF was stronger than the correlation between medium OH and clonogenic SF, which means equivalent radiation for intracellular ROS could be considered as common index for the bioeffects of radiation and plasma. In this study, we quantitated plasma dose in terms of equivalent radical production compared with radiation dose. We concluded that plasma treatment can be estimated by quantitating the equivalent radiation dose.

Keywords: Equivalent radiation dose, Plasma medicine, Non-thermal plasma, Plasma dose,

Student Number : 2013-23185

CONTENTS

List of tables

List of figures

CHAPTER 1

INTRODUCTION

1.1 NON-THERMAL PLASMA TREATMENT

Plasma is a fourth state of the matter in which ionized gas exhibits a collective behavior when long-range electric and magnetic fields prevail over short-range forces. Plasmas can be generated by heating or subjecting neutral gas to a strong electromagnetic field to the point where ionized gaseous substance becomes highly conductive. Plasma is classified into thermal plasma and non-thermal plasma based on the temperature and density of the plasma states. Thermal plasmas show that heavy particles (positive ions and neutral atoms) and electrons at the same temperature which is generally reaching up to thousands of kelvins. On the other hand, non-thermal plasmas or cold plasmas are not in thermodynamic equilibrium, which electrons have a higher temperature rather the temperature of heavy particles.

In the last decade, non-thermal plasma has been studied in medical treatments, such as microorganism deactivation, wound healing, blood coagulation, dental cavity treatment, angiogenesis suppression, and cancer treatment [1-5]. The first application of plasma treatment was based on the thermal effect of plasma in the 1990s. High temperature and heat generated by Argon Plasma Coagulator (APC) were used for the treatment of tissue removal such as hemostasis by cauterization [6-8]. APC could provide alternatives to hot metal contact electrocautery in which applies controlled heat to tissue surface by passing sufficiently high current through the tissue layer. Another application was to apply low-temperature plasma to treat the wounds of the injured and to sterilize biotic and abiotic surfaces in US Air Force Office of Scientific Research (AFOSR) [9,10].

A study revealed that wound healing effect was due to the plasma-generated Nitric oxide (NO) which enhanced phagocytosis and accelerating the proliferation of tissue [11].

Stoffels et al. reported that non-thermal plasma was used to detach mammalian cells without inducing necrosis and induce apoptosis without causing thermal/electric damage to the cells [12]. These early achievements raised attention and led many laboratories to investigate the biomedical applications of non-thermal plasma. Figure 1 shows a timeline graph of some important milestones in the development of the application of non-thermal plasma. Today, the field of plasma medicine covers several applications in biology and medicine. These included [1,3,9,10]:

- Sterilization, disinfection, and decontamination
- wound healing
- Plasma dentistry (tooth bleaching)
- Plasma oncology (cancer treatment)

Most important parameters of plasma medicine are the radicals generated from the gaseous phase of plasma. Reactive oxygen and nitrogen species (RONS) are known to play several roles [9,10]. RONS affect the cells including from proliferation to cell death are applied for medical treatment. Recently, most of studies have focused on the anti-cancer treatment effect because cancer cells were induced cell death selectively or volume reduction of tumor tissue was induced [13,14]. Cancer cells with increased oxidative stress are likely to be more vulnerable to damage by exogenous production of ROS and the cellular mechanisms of cancer cell death have been reported through several studies.

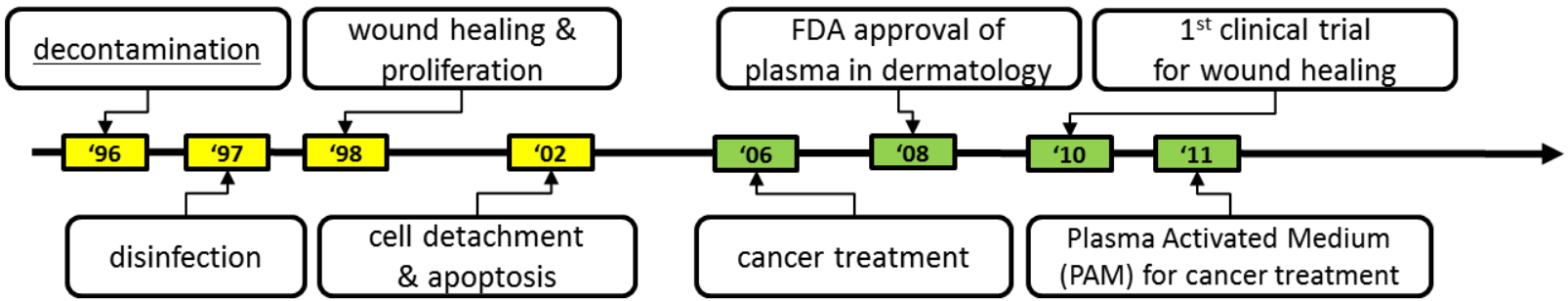

Figure 1.1 A timeline graph of milestones in non-thermal plasma medicine.

1.2 Object of the study

The non-thermal plasmas were generated from various discharge devices including floating-electrode dielectric barrier discharge, atmospheric pressure plasma jet (APPJ), and plasma needle [1,4].

Non-thermal plasma affects cancer cells by generating diverse mediators including charged particles, reactive oxygen species (ROS), reactive nitrogen species (RNS), UV, and electric fields [1,13-17]. In medical uses, plasma is prescribed at low intensities and thus the physical species (UV, heat, electromagnetic field) have minimal effect or negligible [15-17]. Earlier studies explored biological mechanisms behind the effectiveness of RONS in cancer treatment with plasma and found that the plasma-generated ROS mostly contributes to accumulating raising the oxidative stress and finally inducing cell death [18-24]. While ROS are known to induce cell death, RNS are known to rarely induce cell death. A study reported that chemical prescription of 100 times stronger NO produced by plasma could not induce any growth inhibition of tumor tissue [23], and other studies reported RNS had minor effect on cell death.

Non-thermal plasma and ionizing radiation operate a common pathway for cell-killing effect, that is, ROS production. Non-thermal plasma generates the OH radical in gaseous form and transfers the radicals to the medium [25-27]. The OH radical plays an important role in plasma medicine because of its higher oxygen potential and stronger disinfection power as compared with the other oxidative species [28, 29]. Notably, the OH radical is a major mediator for DNA damage in cells under exposure to radiation of low linear energy transfer (low-LET radiation), such as X-rays and γ-rays [30,31]. As a common physicochemical factor produced in plasma and radiation treatments, the OH radical production can indicate the

extent of cellular exposures to plasma and radiation. Therefore, in this study, We set OH radical as main factor and quantitated OH radical production in both experiments.

For comparing low-LET radiation and plasma in terms of OH radical production, low-LET radiation can penetrate a medium, while plasma cannot penetrate it and mostly produce radical at the surface of the medium. In this study, we conducted experiments in both radiation and plasma treatments on medium containing the cell. X-ray generates homogeneous radical production inside and outside the cells, while plasma mostly generates gaseous form of OH radical at the medium surface. We analyzed the pathway in which plasma-generated OH induced intracellular damage to solve this problem.

Plasma treatment is generally prescribed by setting the operational parameters of the source device with regard to gas combination, gas-flow rate, applied voltage, and treatment duration without concept of dosimetry. It contrasts with radiation treatment which prescribed in terms of radiation dose. The parametric choices of plasma reactor were normally based on the empirical results in formal studies. In this study, we evaluated the effects of individual parameters, such as gas-flow rate, applied voltage, and treatment duration, of a plasma production device on the radical production and clonogenic death of in vitro cells. We also sought the radiation dose levels that cause the comparable radical productions and clonogenic cell deaths with the plasma exposures under different parametric combinations in operation of a plasma source device. We defined comparable radiation dose as the *equivalent radiation dose*. The concept of *equivalent radiation dose* for non-thermal plasma can be used for calculation and assessment of the non-thermal plasma dose in therapeutic approach.

CHAPTER 2

THERORETICAL BACKGROUND

2.1 Principles of non-thermal plasma treatment

2.1.1 Interactions between non-thermal plasma and cells

The interactions between non-thermal plasma and cells are composed of various physical and chemical factors [9,10,13-15]. Figure 2.1 shows a schematic illustration for the interaction between non-thermal plasm and cells. Physical factors include Ultraviolet (UV), heat, electromagnetic field and chemical factors include various reactive oxygen species (ROS) and reactive nitrogen species (RNS) that are generated in the gas phase of non-thermal plasma.

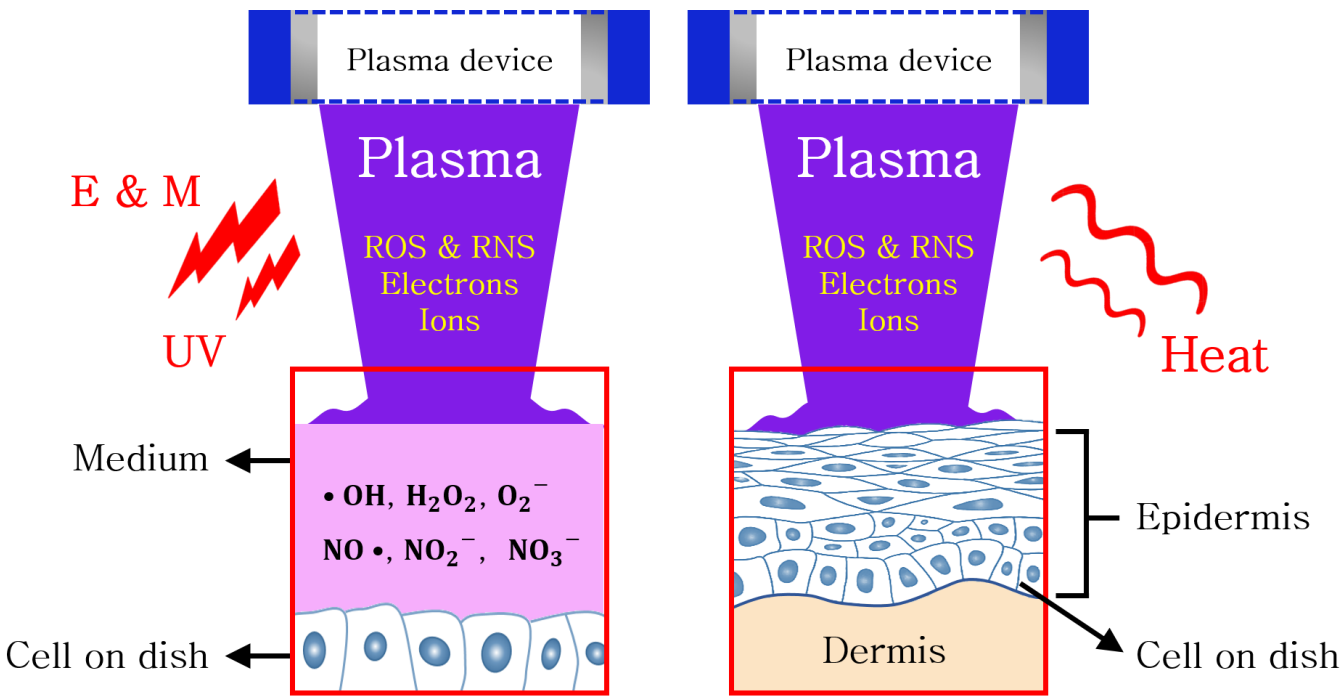

Figure 2.1. A schematic illustration of interaction between non-thermal plasma and cells in vitro and in vivo. The dissolved species in medium have been estimated to play major role in vitro. On the other hand, non-thermal plasma has been applied to inhibit tumor growth in vivo.

Lin A. et al reported that physical factors such as UV, heat, electromagnetic field is negligible for the interaction between plasma and cell [24]. Table 2.1 shows treatment condition to understand contribution of plasma components on cell death. By dipping electrode in medium (No. 2 in Table 2.1), only electromagnetic field from plasma was applied to the cells, and there is not any effect on cell viability. In the presence of the quartz barrier (No. 3 in Table 2.1), only UV was applied to cells and other components were ignored and one third of total cell death was increased. UV is known to trigger cell death by penetrating cells and damaging DNA, and also generate intracellular ROS including hydroxyl radical and hydrogen peroxide [32,33]. However, low dose of non-thermal plasma is usually applied for medical use, UV is estimated to have low or no direct biological effect [15]. Therefore, we neglected the effect UV on cells for this study.

Non-thermal plasma are generated by applying energy into the production of energetic electrons whereas the ions and atoms remain in low energy states resulting in a low plasma temperature. Excited and ionized atoms or molecules interact with other atoms or molecules of the working gas and with surrounding air resulting in the generation of reactive species with biological potential. Therefore, thermal damage is neglected in this study. Also previous study reported that the He-APPJ used in this study was shown operated at room temperature and there was non-thermal effect on the target [34].

Table 2.2 shows biologically important reactive species generated by non-thermal plasma. RONS are generated in large concentration in plasma-liquid interaction, and reactive species are transferred to liquid phase and play a major biological role [35]. Many studies reported that ROS plays a major role rather than RNS plays a minor role. Several studies reported that plasma generated hydrogen peroxide (H_2O_2) concentration in

medium is correlated strongly with the cell viability [36-39]. On the other hand, Reuter S. et al reported ROS-dominated plasma decreased cell viability more than RNS-dominated plasma [40]. Other studies still reported that RNS is minor anti-cancer factor in vitro studies [41,42]. These evidences suggest plasma-generated ROS including OH radical, H_2O_2 are dominant factors in anti-cancer mechanisms of plasma medicine.

Table 2.1. Summary of conditions used to isolate and remove plasma components [24].

No.	Treatment condition	Present factors	Absent factors	282 mJ Cell death [%]	705 mJ Cell death [%]
1	Direct uniform DBD−Plasma in air	E−field, UV, charges, neutrals	−	50	80
2	Electrode dipped in media	E−field	UV, charges, neutrals	0	0
3	Uniform DBD with quartz barrier	UV	E−field, charges, neutrals	16	23
4	Uniform DBD−plasma with mesh barrier	Long lived neutrals, UV	Global E−field, Charges, Short−lived neutrals	24	35
5	Uniform DBD plasma in oxygen	ROS, Charges, E−field, UV	Other neutral species	58	85
6	Uniform DBD plasma in nitrogen	RNS, Charges, E−field, UV	Other neutral species	0	0

Table 2.2. Reactive species generated by non-thermal plasma

Reactive oxygen species (ROS)	Reactive nitrogen species (RNS)
Hydroxyl radical (•OH) [9-16,35]	Nitric oxide (•NO) [11,35]
Super oxide (O_2^-•) [35]	Nitrogen dioxide (•NO_2) [35]
Singlet oxygen ($^1O_2$) [35]	Nitrogen trioxide (•NO_3) [35]
Ozone (O^3) [35]	Peroxynitrite ($ONOO^-$) [35]
Hydrogen peroxide (H_2O_2) [35]	
Organic radicals (RO•, RO_2•)	

2.1.2 Production of hydroxyl radical in non-thermal plasma

The hydroxyl radical (OH radical) can be produced in non-thermal plasma through a variety of reactions [43]. Table 2.3 shows the list of reactions generating OH radical and the plasma conditions for typical rates. The OH radical can be produced by dissociation which is driven by electron collision and attachment reactions, ion-electron and ion-ion recombination reactions, thermal dissociation and collisional dissociation reactions with other radicals and metastable. Vibrational excited H_2O molecules can be participated to dissociate for producing OH radical. Figure 2.2 shows major reaction rates from the literature below [44].

The production of OH radical is dependent on these parameters.

- The gas temperature (T_g)
- The electron temperature (T_e)
- The ionization degree
- The electron density (n_e)
- The vibrational temperature
- The gas composition

From table 2.3, it is shown that different plasma sources span a large parameters of T_e, T_g, and n_e. The ionization degree ranges from 10^{-2} to 10^{-8}, and gas temperatures are ranged from 300 to 6000 K. The electron temperatures of steady-state plasmas are approximately from 1 to 2 eV. The large variety of plasma properties, which is shown in Table 2.4, dominant radical production mechanism significantly change between different discharges or even within the same discharge in the case of transient discharges, which consist of ionizing phase and a recombining phase separated in time [45].

Table 2.4 shows some typical plasma properties for glow

discharge, dielectric barrier discharge (DBD), and streamers. The electron energy is range from 1 to 10 eV, therefore, production of OH radical is mainly due to dissociative recombination after the pulse (in the case of a pulsed duration of the order of 100ns). Electron-induced dissociation can induce OH radical production to the surrounding edge of the plasma, for which dissociative recombination processes locally produce the radicals. Therefore, the most OH radical is produced by the electron-impact dissociation of H_2O and H_2O^+ molecules.

Table 2.3 Dominant reactions of producing OH radical from the literature

Reaction	Rate coefficient ($cm^3\ s^{-1}$)	Remark	Ref
Thermal dissociation			
$H_2O + H_2O \rightarrow OH+H+H_2O$	10^{-20}-10^{-14}	T_g=2500-5000 K	[46]
Electron dissociation			
$H_2O+e^- \rightarrow OH+H+e^-$	10^{-12}-10^{-10}	T_e = 1-2 eV	[47]
Electron-ion dissociative recombination			
$H_2O^+ + e^- \rightarrow OH+H$	10^{-10}	T_e = 1 eV	[48]
$H_3O^+ + e^- \rightarrow OH+H_2+e^-$	10^{-7}	T_e = 1 eV	[49]
Dissociative attachment			
$H_2O+e^- \rightarrow OH+H^-$	10^{-12}-10^{-11}	T_e=1-2 eV	[47]
Water ion hydration			
$H_2O^+ + H_2O \rightarrow H_3O^+ + OH$	10^{-9}		[50]
Positive-negative ion recombination			
$H^- + H_2O^+ \rightarrow OH+H_2$	10^{-13}	T_g~300 K	[51]
$H^- + H_3O^+ \rightarrow OH+H_2+H$	10^{-13}	T_g~300 K	[49]
Dissociation by radicals and metastables			
$O(^1D) + H_2O \rightarrow OH+OH$	10^{-16}	T_g ~ 300 K	[52]
$O+H_2 \rightarrow OH+H$	10^{-17}-10^{-11}	T_g=300-3000 K	[53]
$H+O_2 \rightarrow OH+O$	10^{-21}-10^{-11}	T_g=300-3000 K	[53]
$H+O+M \rightarrow OH+M$	10^{-14}	T_g=300-3000 K	[46]
Dissociation by vibrational excitation			
$H_2O+H_2O^* \rightarrow OH+H+H_2O$	10^{-14}	T_v = 0.5 eV T_g=300 K	[54]

Table 2.4 Overview of some estimates of pulsed discharge properties and OH radical generation rate with plasmas [43]

T_e	n_e	T_g (K)	Generation (cm^{-3})	Discharge type
1	10^{14}	300	10^{14}	Glow
1	10^{15}	300	10^{16}	Glow−like
2	10^{15}	300	10^{16}	Glow−like
3	10^{14}	300	10^{16}	DBD
10	10^{14}	300	10^{17}	Streamer

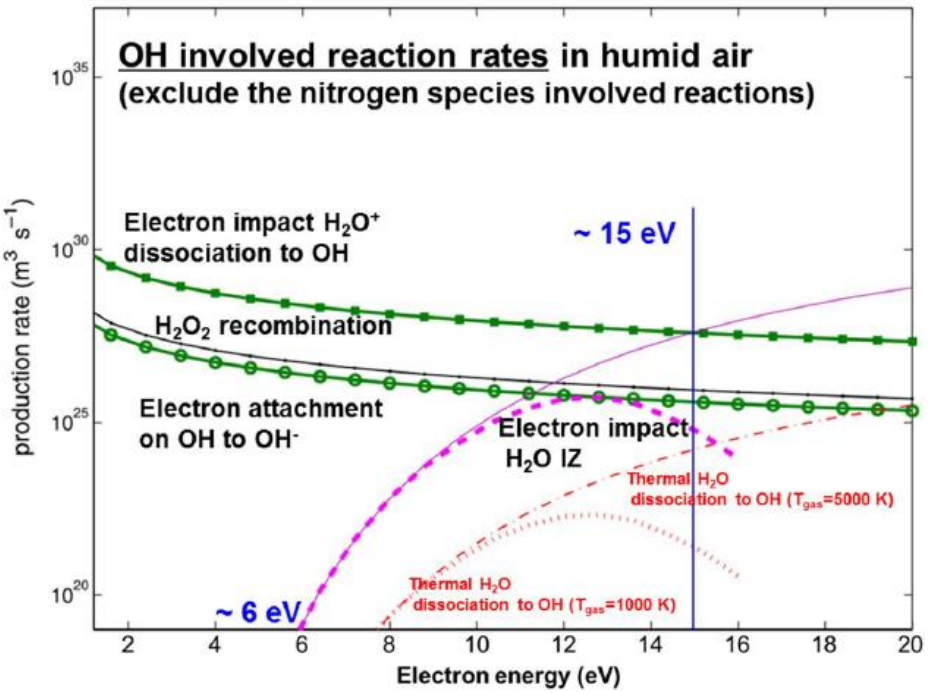

Figure 2.2 Major reactions of generation or loss of OH radical with electron energy. H_2O^+ dissociation is dominant for producing OH radical at electron energy below 15 eV. Dominant loss of OH radical is reaction of H_2O_2 recombination at electron energy 10 eV. [44]

2.1.3 OH radical production of APPJ

Atmospheric pressure plasma jet (APPJ) is used for discharge of non-thermal plasma in this studies. Helium (He) and Argon (Ar) gas are widely used as working gas. Helium gas was used in this study because He has higher metastable energy (20.96 eV) than that of Ar (11.5 eV) [55]. Figure 2.2 is a schematic diagram of DBD-like APPJ reactor structure used in this study. Working gas are guided into dielectric tube for which ring electrode is located around the tubes and HB electrode is at center. High electric field between a pair electrodes induces breakdown of the discharge gas and the plasma propagates along the tube.

The main reactions for producing OH radical by He-APPJ is listed on Table 2.5 [56]. The electron impact dissociation of H_2O molecule is the predominant reaction and the recombination of H_2O^+ by $O(^1D)$ is main reaction to produce the OH radicals. Also, as the helium plasma flows downstream, nitrogen atoms in ambient air are entrained into helium gas flow, which is attribute to the increase electron density through Penning ionization [57].

$$He + e \rightarrow He^* + e$$
$$He + e \rightarrow He^m + e$$
$$He^* + N_2 \rightarrow N_2^+ + He + e \text{ (Penning ionization)}$$

OH radicals are generated various area from APPJ (shown in figure 2.3) [58]. First, the OH radicals can be produced in the plasma plume with the donut shape at outer tube. The others can be produced inside the tube and flowed downstream by gas flow. If plasma interacts with target containing H_2O, OH radical can be produced by discharge along the surface [59,60]. Evaporation of water increases OH radical production by the dissociation of H_2O molecules.

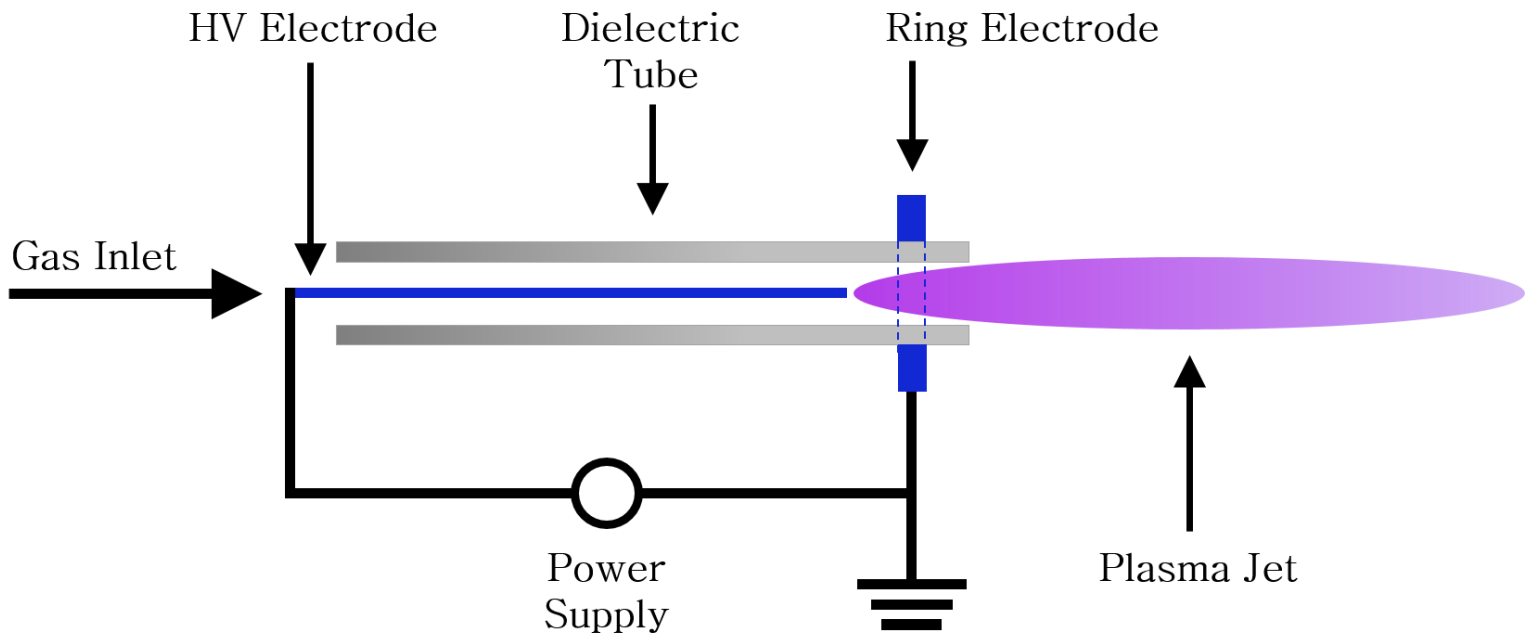

Figure 2.3 A schematic of a DBD-like plasma jet. High voltage applied to pin at center and a grounded ring at the edge of the dielectric tube. Gas is injected from the top of the tube with laminar flow

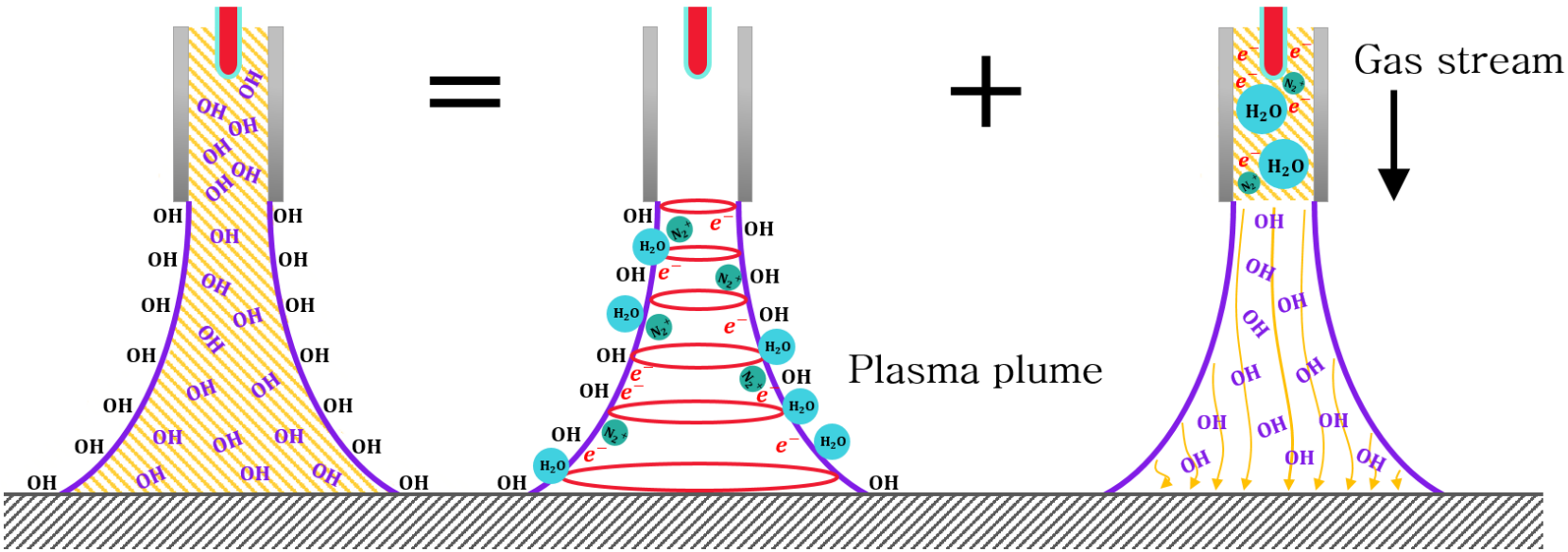

Figure 2.4 A schematic diagrams of the OH production mechanisms of APPJ. A donut shape of OH radical results from both the OH radical generated by plasma bullet outside the tube and the OH radical generated inside the tube flowing with gas. [58]

Table 2.5 Helium−H_2O reaction mechanism used in this study [56]

Helium−air−H2O chemistry (molecules−meters−kelvin)		
Reaction	Rate coefficient (cm^3s^{-1})	ref
$e^- + H_2O \rightarrow 2e^- + H_2O^+$		[61]
$e^- + H_2O \rightarrow H + OH + e^-$		
$e^- + H_2O^+ \rightarrow H + OH$	7.11×10^{-4}	
$e^- + H_2O^+ \rightarrow H + H + O$	3.1×10^{-4}	
$OH + H + M \rightarrow H_2O + M^\dagger$	4.3×10^{-31}	
$O(^1D) + H_2O \rightarrow OH + OH$	2.2×10^{-10}	
$OH + OH \rightarrow O + H_2O$	2×10^{-12}	
$O + OH \rightarrow H + O2$	3.32×10^{-11}	
$O + H + M \rightarrow OH + M^\dagger$	1.62×10^{-39}	[62]
$H + O_2 \rightarrow OH + O$	3.55×10^{-22}	
$OH + M \rightarrow O + H + M^\dagger$	4.15×10^{-82}	
$H_2O + O \rightarrow OH + OH$	2.34×10^{-15}	
$He^+ + H_2O \rightarrow H_2O^+ + He$	6.05×10^{-12}	
$He^* + H_2O \rightarrow e^- + H_2O^+ + He$	6.6×10^{-10}	
$He_2^* + H_2O \rightarrow e^- + 2He + H_2O^+$	6×10^{-10}	

†Species M in reaction represents third−body species.

The measured radial distribution and estimated surface temperatures of He-APPJ from the previous study are shown on Figure 2.5 [34].

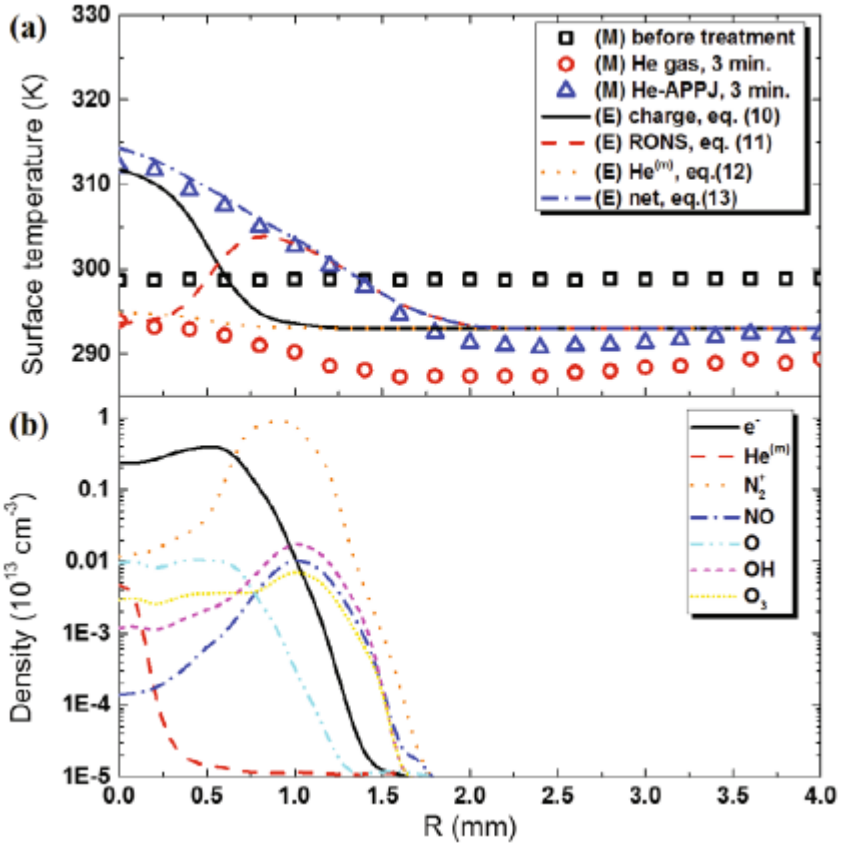

Figure 2.5 (a) Results and estimated value of Surface temperature distribution. (M) is measured value & (E) is estimated value, (b) Particle distribution on agar surface [34]

2.1.4 Pathways of intracellular ROS production by plasma

The DMPO-OH signal intensity corresponds to the concentration of OH radicals in the cell culture medium. Notably, ROS molecules are cell-threatening when they are produced inside the cells [62-65]. Low-LET radiations, such as X-rays, are penetrating matters and the OH production by X-ray exposure would be uniform over the intra- and extra-cellular regions. However, plasma treatment leads to produce OH radicals mostly at medium surface. The OH radical produced near the medium surface hardly reach the cells due to their short mean diffusion length. Nevertheless, cold plasma has been report to induce damage in from organelles to DNA in nucleus [65-67].

Recombination of extracellular OH radical

Concentration of OH radicals at very close to medium surface is very high (order of 10^{15} cm^{-3}) [25]. Highly reactive OH radicals can be combined to form gaseous H_2O_2 molecules. Due to the high value of Henry's constant, these gas phase H_2O_2 can diffuse into the medium to form liquid phase H_2O_2. Otherwise, highly accumulated OH population at medium surface are balanced by the loss of diffusion and recombination. the maximum diffusion length inside the water was estimated to be 1.67 μm in the reference [68]. Recombination of H_2O_2 reaction can occur within the small diffusion length.

$$\bullet OH + \bullet OH \rightarrow H_2O_2,$$
$$(k = 1.78 \times 10^{-11}\ cm^3 s^{-1})$$

Transport of H_2O_2 into cells

Several studies reported the mechanism in which extracellular H_2O_2 are transported into the cells through membrane proteins [69–75]. A recent study proved that aquaporin 8 expressed on the cell membrane played as the diffusion channels of non–thermal plasma–generated H_2O_2 [76]. And plasma–generated superoxide (O_2^-) can enter the cells by diffusion [77]. Several studies proved that extracellular H_2O_2 and O_2^- were diffused into the cells and contributed to the increase of intracellular ROS in the treated cells [18,69,78].

Pathways of inducing intracellular ROS

A study proposed a mechanism in which plasma induces intracellular OH radical production although plasma produces most radicals outside the cells [79]. The relatively stable H2O2 molecules play the major oxidant in plasma treatment [21,80–82]. Proteins, such as ferritin and ferroportin, expressed in cells are able to catalyze H2O2 into OH radical by Fenton reactions.

$$H_2O_2 + O_2^- \xrightarrow{Fe^{2+}} HO^- + \bullet OH + O_2$$

The metal–catalysed reaction which generates OH radicals from H_2O_2 and O_2^- has ability to produce high local concentration of OH radical. A clustered damage may result from the activation of H_2O_2 by transition metal ions located close to DNA [83].

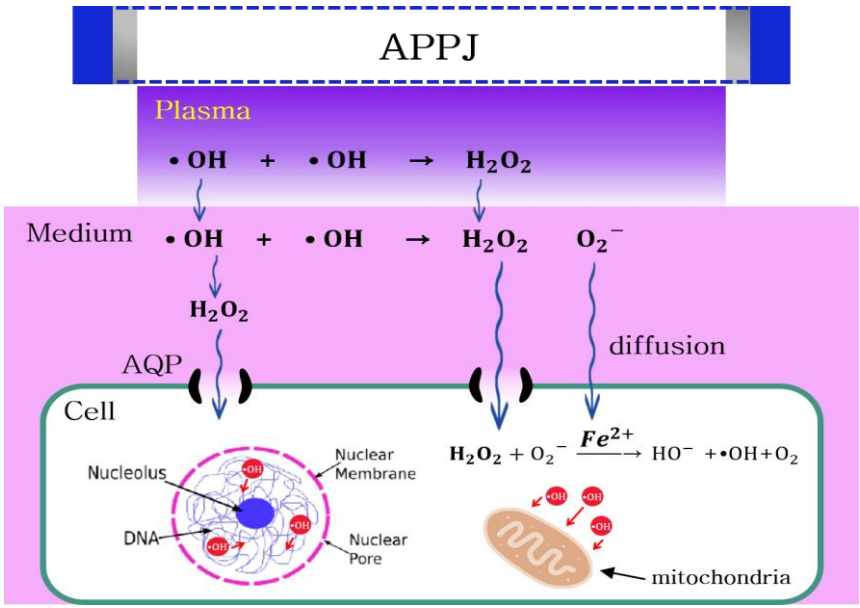

Figure 2.6 Whole scheme of the plasma-generated OH radical for inducing cell death. Non-thermal plasma discharged by APPJ interacts with medium and concentrate OH radical at the medium surface. H_2O_2 generated by recombination of OH can diffuse relative long distance in medium. H_2O_2 can diffuse inside the cell through aquaporin and O_2^- can diffuse cell membrane and both species generate intracellular OH by Fenton reaction.

2.2. Hydroxyl radical production by low LET radiation

If a cell is exposed to radiation, the probability that radiation interacts with DNA molecules is very small since the critical components which are very close to DNA molecules make up a small part of the cell. On the other hand, water make up most of the cell's volume, and radiation has a higher probability to interact with water molecules in the cell. Direct effect occurs when radiation interacts with cellular DNA molecules and transfers energy to break DNA band, and indirect effect occurs when the reactive species are generated by interactions of the primary radiation and secondary electrons very close to DNA molecules. Indirect effect is dominant when low linear energy transfer (LET) radiation interacts with a cell.

When X-ray radiation interacts with water molecules, water excited molecules or ions, and free radicals are generated. Figure 2.5 shows the initial reactions in below. Among them, OH radical is one of the most important species since massive OH radical production is known to responsible for the majority of radiation induced DNA damage [63,64,83].

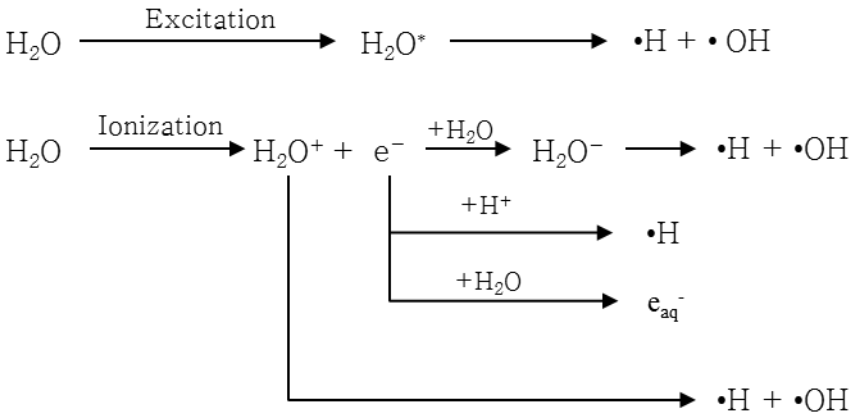

Figure 2.7 Radical products as the result of water radiolysis. After the energy deposition (in the physical stage, 10^{-15} s), the excited or ionized molecules are dissociated into OH radical, H radical, and e_{aq}^- (in the physicochemical stage, $10^{-16}-10^{-12}$ s) [84]

2.3. ESR spectrometry of the OH radical with spin trapping method

ESR spectrometry is a method for detecting materials with unpaired electrons. The ESR spectrometry detect free radical directly by measuring the interaction of unpaired electron spins with an external magnetic field [85]. When an unpaired electron is aligned with the magnetic field, the electron's magnetic dipole moment aligns either parallel (ms=−½) or anti−parallel (ms=+½) to the magnetic field. Each alignment corresponds to a specific energy level with slightly more electrons ended up in the lower energy level due to Maxwell−Boltzmann distribution. The energy gap between the two states is directly proportional to the external magnetic field and can be expressed as:

$$\Delta E = g_e \mu_e H_o$$

(g_e: g−factor, μ_e: Bohr magneton, Ho: External B field)

An unpaired electron moving between these two energy levels either absorb or emit electromagnetic energy. When an external microwave (frequency ν) is imposed and $h\nu = \Delta E$, resonance happens.

The OH radical is very unstable and has short half−life due to high reactivity, direct detection of OH radical is impossible at room temperature [86−89]. The spin trapping technique which a nitrone or nitroso compound reacts with target involves the addition of the reactive free radical across the double bond of a diamagnetic spin trap to form more stable radical adduct. Figure 2.6 shows spin trap adduct DMPO−OH used for detecting OH radical. Phenyl−tert−butyl nitrone (PBN) and 5,5−dimethyl−1−pyrroline−N−oxide (DMPO) are diamagnetic molecules (S=0), however, PBN−OH or DMPO−OH are paramagnetic molecules (S=1/2) which can be detected by EPR spectrometer.

In this study, we chose the DMPO as spin trap material because DMPO-OH is appropriate for quantitative measurement of OH radical. The DMPO-OH adduct has a relatively long half-life (870s). The following step is measurement of DMPO-OH generated by X-ray exposure or non-thermal plasma treatment with ESR spectrometer. The double integration was conducted on ESR spectrum to calculate area from the first derivative of the absorption signal.

(i) Prepare DMPO-OH containing medium.

(ii) Treat the medium with desired condition.

(iii) Measure the signal intensity of DMPO-OH adduct.

(iv) Estimate the intensity by integrating the signal.

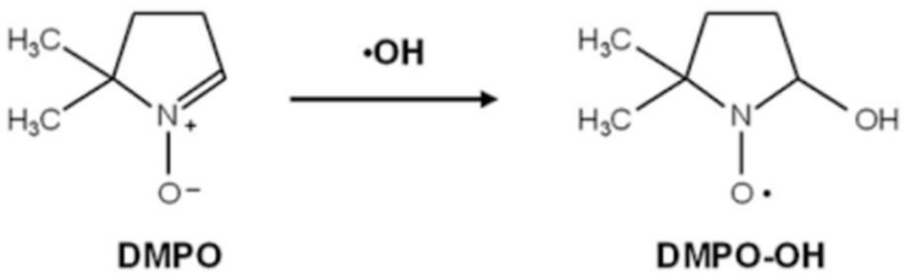

Figure 2.8 Chemical constitution of DMPO and DMPO-OH for ESR measurement

CHAPTER 3

MATERIALS AND METHODS

3.1 X-ray irradiation

The X-ray irradiation of mediums and cells was conducted in the hard X-ray beam facility. The X-ray beam is generated from a beam tube (450-D08, YXLON, Hamburg, Germany), when tungsten target is hit by the electrons accelerated at the operating anode. The bremsstrahlung X-rays at below 20 keV was filtered by a 3-mm thick aluminum plate fitted over the 5 mm-thick beryllium window.

In this study, we operated the X-ray tube at 350 kVp and 10 mA. The dose rate was 3.68 Gy/min when the distance between beam exit to target was set to 40 cm. Figure 3.1 presents the schematic diagram of the hard X-ray beam facility.

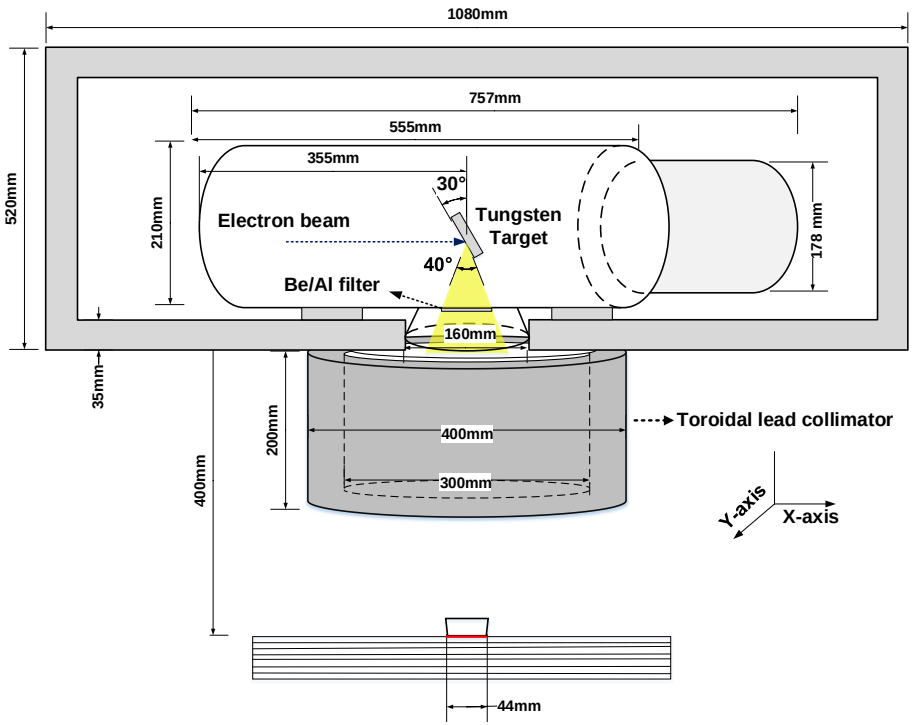

Figure 3.1. A schematic diagram of X-ray generator for irradiation. Cell dish was placed on a phantom made of tissue-equivalent material.

3.2 Atmospheric Pressure Plasma jet (APPJ)

Figure 3.2 presents the schematic view of APPJ for generating non-thermal plasma into the medium. A alumina tube with an outer diameter of 0.67 mm is surrounding a tungsten electrode at the center of a coaxial quartz guiding tube. Helium gas was injected was discharge gas into the gap between the alumina and the quartz tube. The gas flow rate was fixed as 2 standard liters per minute (SLPM) by using a mass flow controller (TN2911V-4S, Allen, Texas, USA). A ring-shaped grounded copper electrode was positioned at the 1mm above at end of the quartz tube. The plasma was discharged by varying the voltage applied to the tungsten electrode with a function generator (33220A, Agilent, Santa Clara, CA, USA) at 20 kHz and a voltage amplifier (20/20C, Trek, New York, NY, USA) at 2000 times amplification. The applied voltage was set as 5 kVp, 7 kVp, and 9 kVp.

The 10 mm-diameter TubeOne® microcentrifuge tubes (S1620-2700, STARLAB, Hamburg, Germany) were filled with 2.0 ml culture medium containing 2x105 cells. The distance between the nozzle of APPJ device and the medium surface was fixed at 20 mm. The plasma fluence over the cells and culture medium was further controlled by varying the duration of plasma treatment.

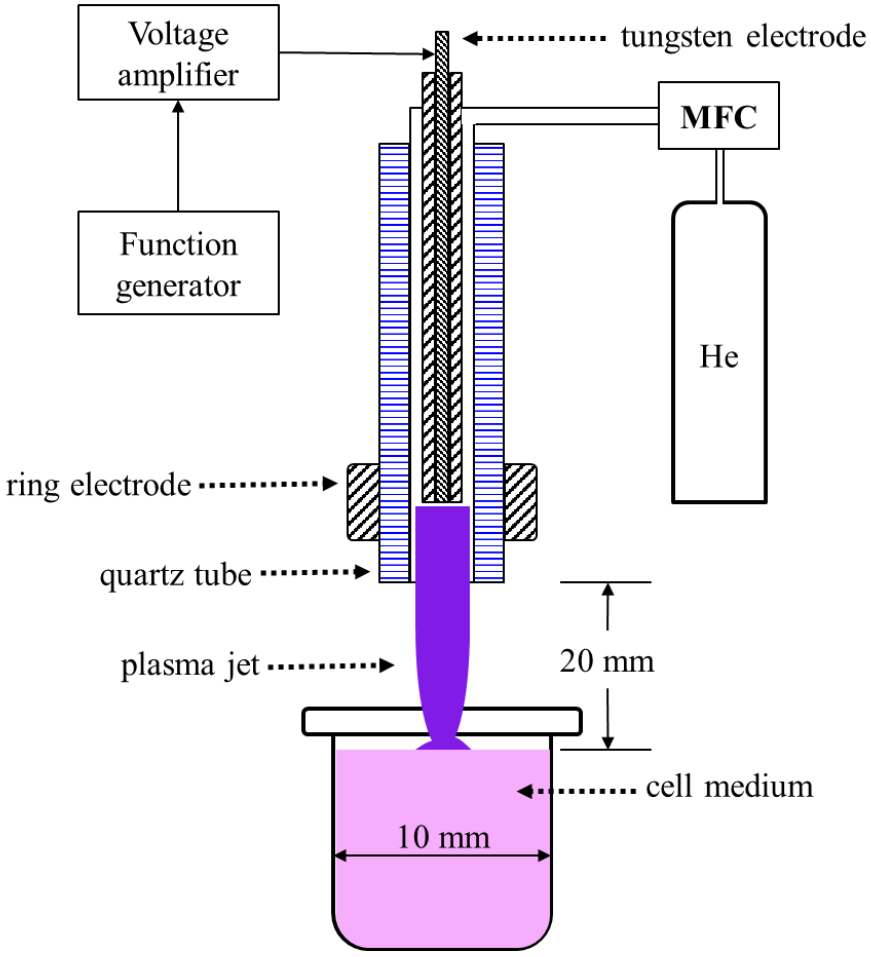

Figure 3.2 A schematic of APPJ injection into cell culture medium. The helium gas-flow rate is controlled by a mass flow controller. The high electric field produced between two electrodes induces breakdown of the helium gas. Then, the plasma propagates along the tube over the cell culture medium.

3.3 Measurement of DMPO-OH signal intensity

The spin trap of 5,5-dymethyl-1-pyrroline-N-oxide (DMPO, D5766, Sigma Aldrich, St. Louis, MO, USA)) was used for measuring concentration of OH radical produced in medium. DMPO formed radical adduct with OH radical and it would maintain a rather long half-life about 870 s.

DMPO was dissolved in DMEM (Gibco) supplemented with 10% (v/v) heat-inactivated FBS (Gibco) before treatment. The medium containing 100 mM DMPO was placed in the 2.0 ml TubeOne® microcentrifuge tubes (S1620-2700, STARLAB, Hamburg, Germany) and exposed to either X-rays or plasma. After irradiation or plasma treatment, the samples were analyzed by ESR spectrometer (JES-TE200, JEOL, Tokyo, Japan) at NICEM in SNU. ESR measurement was taken 6 minute after X-ray exposure or plasma treatment.

Each sample was imbibed by a glass capillary (40 μl) and detected in the resonator cavity at room temperature. All measurements were performed in triplicate for each condition, and the operation time was kept strictly the same. A manganese signal was used for standardizing the external signal. The parameters of the ESR spectrometer was set as the following.

- Central field: 341.0 mT ± 10 mT
- Sweep width: 20 mT
- Microwave frequency 9.42 GHz
- Microwave power: 1.0 mW
- Sweep time: 2 min
- Amplitude: 200-fold (amplitude)

3.4 Cell line and cell culture methods

MECs (CRL-2161, ATCC, Manassas, VA, USA) were cultured in T-25 flask (Nunc, Roskilde, Denmark) containing Dulbecco's modified eagle medium (DMEM) (Gibco, Grand Island, NY, USA) supplemented with 10% (v/v) heat-inactivated fetal bovine serum (FBS) (Gibco). All cells were incubated at 37 ℃ in a humidified incubator (MCO-230ALC, Panasonic, Gunma, Japan) with 10% CO2. Before exposure to X-ray or plasma, cells were washed with phosphate-buffered saline (Invitrogen, Carlsbad, CA, USA) and prepared into single-cell suspensions with TrypLE Express (Gibco). According to the product information sheet, this cell line was recommended to exchange medium every three days.

3.5 Detection of intracellular ROS concentration

Cells were incubated with 50 μM H_2DCF-DA (ab113851, Abcam, Cambridge, UK) in culture medium for 30 min at 37 ° C and 10% CO_2. The H_2DCF-DA-loaded cells were exposed to either X-rays or plasma and then incubated for 30 min.

The intracellular ROS assay is followed by three steps:

(ⅰ) Cells are incubated with medium containing DCFH-DA for 30 min. DCFH-DA was freely diffused into the cells.
(ii) After diffusion into the cell, DCFH-DA is deacetylated by cellular esterase into a DCFH which is non-fluorescent compound.
(iii) Intracellular ROS oxidize DCFH into a DCF which a highly fluorescent compound detected by fluorescence spectroscopy with maximum excitation and emission spectra of 495 nm and 529 nm, respectively.

The operational setups in applied voltage, helium gas-flow rate, and treatment time of the plasma device were 5 kVp, 2 LPM, and 2 min in condition 1, 7 kVp, 2 LPM, and 1 min in condition 2, and 7 kVp, 2 LPM, and 2 min in condition 3.

Cells were analyzed using a flow cytometry system (FACS AriaTM, BD Biosciences, San Jose, CA, USA) to measure the fluorescence. Cells in suspension pass through a laser excitation beam in single file fashion, and emission fluorescence is measured by an electronic detection apparatus as light scatter and fluorescence intensity. Total 10,000 cells were counted at each treatment conditions for measuring mean fluorescence intensity (MFI). We calculated the ratio of experimental group to control group.

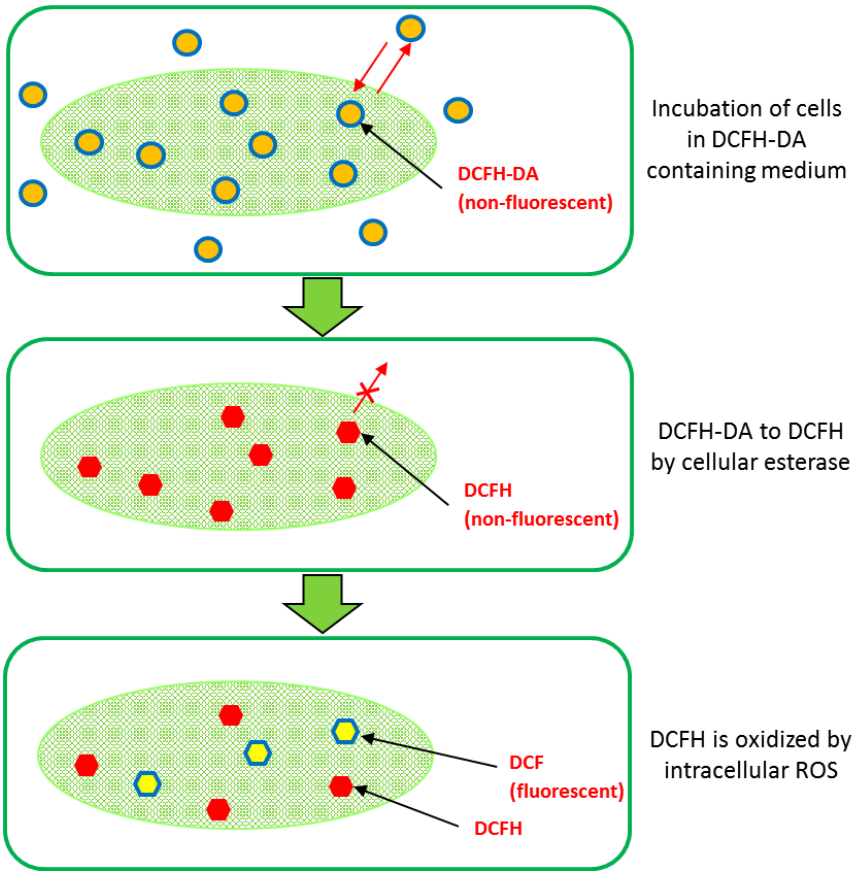

Figure 3.3 A schematic scheme of detecting intracellular ROS concentration of measuring DCF fluorescence.

3.6 ROS scavenging

ROS scavengers were used to investigate the particular ROS effect on cells. Catalase (C1345, Sigma Aldrich), d-mannitol (M4125, Sigma Aldrich) and 2-phenyl-4,4,5,5-tetramethylimidazoline-1-oxyl 3-oxide (PTIO, P5084, Sigma Aldrich) were used to scavenge H_2O_2, OH radical, NO radical, respectively. Each scavenger was added to medium 30 min before treatment.

3.7 Clonogenic assay

Cellular responses to radiation and plasma were determined by clonogenic assay. After exposure to radiation or plasma, cells were plated onto 35 mm culture dishes (Nunc) containing 3 ml of culture medium and incubated for 12 days. During incubation, the medium was replaced with a fresh one every 3 days. At the end of 12-day incubation, the cells were fixed with 70% ethanol and stained with 5% Giemsa solution (Sigma Aldrich). The colonies were counted with the naked eye using a microscope (IX71W, Olympus, Shinjuku, Tokyo, Japan). The colonies of more than 50 cells counted with the naked eye were considered as clonogenic survivors.

When cells are seeded as a single cell suspension in culture medium at low densities, they may grow into colonies. The percentge of colony-forming cells among the seed single cells is the plating efficiency (PE in Eq. (5)). The clonogenic surviving fraction (SF in Eq. (6)) was calculated by dividing the PE after X-ray or plasma treatment by the PE of the control cells.

$$PE = \frac{Number\ of\ colonies\ counted}{Number\ of\ cells\ seeded} \times 100\ (\%)$$

$$SF = \frac{Number\ of\ colonies\ counted\ after\ tretment}{Number\ of\ cells\ seeded \times PE} \times 100\ (\%)$$

3.8 Statistical analysis

All experiments were perfomed in at least thrice, on five separated conditions. The data were fitting using Origin 2017 and presented as mean ± standard error. The standard error was calculated for each set of the experiment.

Student's t-test was performed to evaluate the significance in the difference between observed data. Data were judged to be significantly different from each other when p-value was less than 0.05.

CHAPTER 4

RESULTS

4.1 DMPO-OH production by X-ray irradiation

The intensity of DMPO−OH was measured by electron spin resonance (ESR) spectrometry [90−93]. Figure 4.1 presents the DMPO−OH signals from the cell culture medium exposed to X−rays at 50 Gy. The ESR measurement was made 6 min after X−ray exposure. The 1:2:2:1 ratio of the asterisked four peaks (first, second, third, and fourth from the left) in figure 4.1 is a typical observation of DMPO−OH signals [94]. The outer two peaks indicate the signals of manganese oxide. The ESR signal intensities of DMPO−OH were normalized with those of the Mn_2^+ signals.

The ESR signal intensity increases with increased DMPO−OH concentration [90−93] and thus with increased radiation dose to culture medium. We recorded the average of the second and third peak signal intensities while disregarding the small first and fourth peak [95]. The first and fourth peak were tend to overlapped at low X−ray due to electric noises of ESR spectrometer below 10 Gy area. Figure 4.2 presents the DMPO−OH signal intensities observed after X−ray exposures at 2, 5, 10, 20, 30, 40, and 50 Gy.

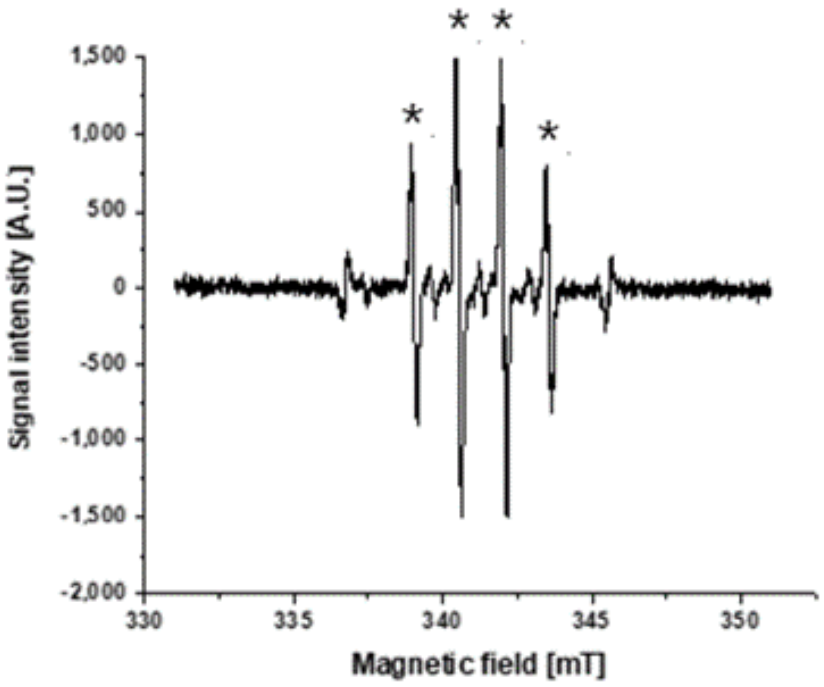

Figure 4.1 DMPO-OH signal intensity of the cell culture medium measured by ESR spectrometer. The asterisked four peaks are DMPO-OH signals and the outer two peaks are the Mn^{2+} markers for data normalization.

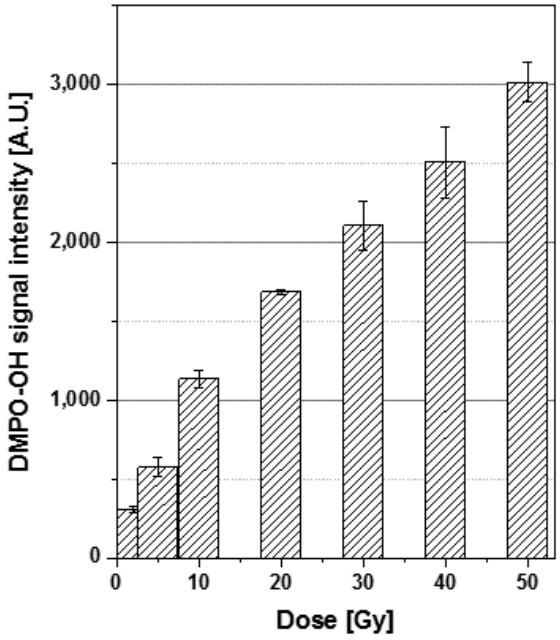

Figure 4.2 Average of the second and third peak value of DMPO-OH signal intensities at 2, 5, 10, 20, 30, 40, and 50 Gy of X-ray irradiation. The signal intensities increases with X-ray doses.

4.2 DMPO-OH production by APPJ treatment

To investigate the effect of the operational parameters of APPJ, each interested parameter was controlled when others were fixed at decided condition. First, to investigate the effect of applied voltage to the production of OH radical, helium flow rate fixed at 2 liters per minute (LPM), and plasma treatment time was fixed at 2 min. As a results, DMPO-OH signal intensity increased proportionally with the applied voltage [Figure 4.3(a)]. The signal intensity and the applied voltage showed a good correlation (R^2=0.99). When the voltage and helium flow rate were fixed at 7 kVp and 2 LPM, respectively, we found out the DMPO-OH signal intensity increased linearly with prolonged duration of plasma treatment in a good correlation (R2=0.99) [Figure 4.3(b)].

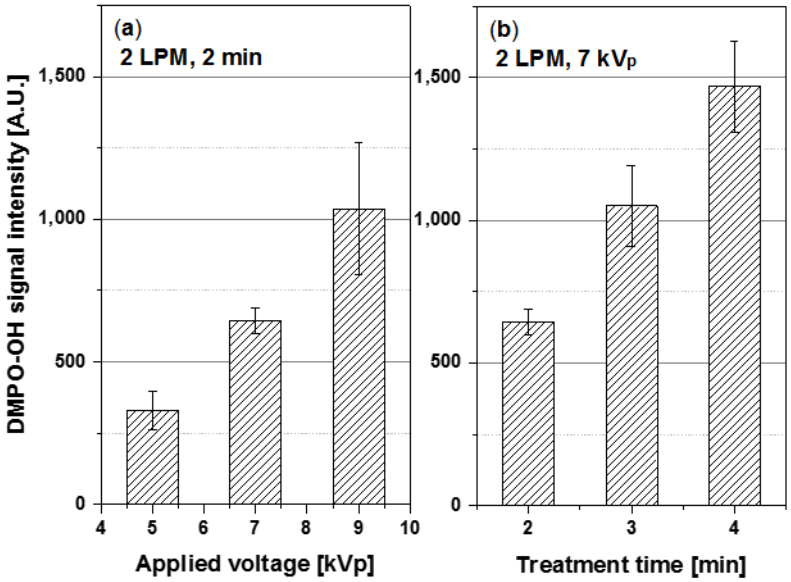

Figure 4.3 DMPO-OH signal intensities after APPJ treatment: (a) from 2 min plasma treatments at the helium flow rate of 2 LPM with the applied voltage at 5, 7, and 9 kVp and (b) from 2, 3, and 4 min treatments at 2 LPM and 7 kVp. Each error bar indicates one standard error of the mean obtained from three independent experiments.

4.3 Intracellular ROS production by X-ray irradiation

The 2′,7’-dichloro-dihydrofluorescein diacetate (H_2DCF-DA) is oxidized by ROS into 2’,7’-dichlorofluorescein (DCF), which DCF is fluorescent compound detected and H2DCF-DA is a non-fluorescent compound. MECs were incubated with H_2DCF-DA containing medium prior to each X-ray and measured the DCF fluorescence intensity by FACS which can differentiate the intracellular ROS concentration from the extracellular one.

In figure 4.5, DCF fluorescence intensity was observed to increase with X-ray dose. As shown in figure 4.4, the DCF fluorescence intensity was increased up to approximately 1750% of that in control. Each data was normalized to the intensity result of control.

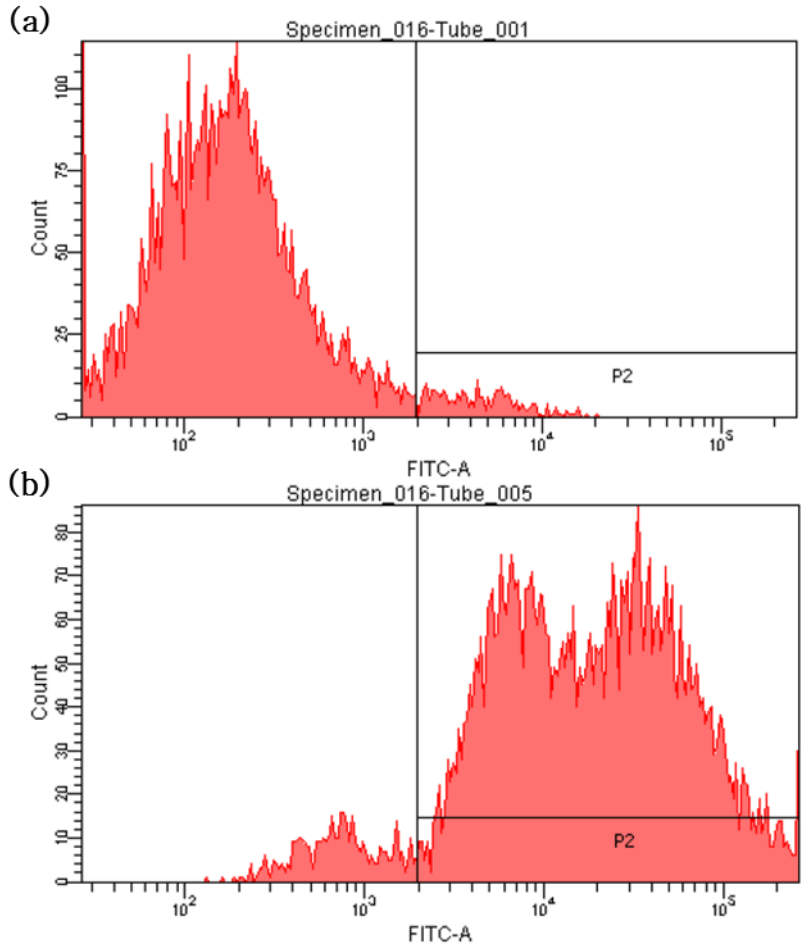

Figure 4.4 Results of DCF intensities measured in MECs after X-ray irradiation. (a) DCF fluorescence intensity of non-irradiated cells (b) DCF fluorescence intensity of 8 Gy irradiated cells

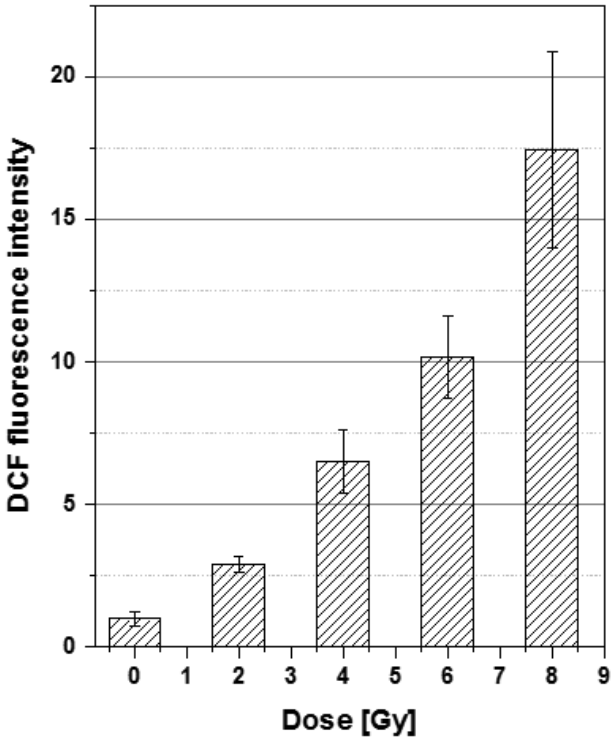

Figure 4.5 DCF fluorescence intensities varying with the X-ray doses in the range from 0 Gy to 2 Gy. Each data was normalized to the control. Each error bars indicates one standard error of the mean obtained from three independent experiments.

4.4 Intracellular ROS production by APPJ treatment

The 2′ ,7’ −dichloro−dihydrofluorescein diacetate (H_2DCF−DA) is oxidized by ROS into 2’ ,7’ −dichlorofluorescein (DCF), which DCF is fluorescent compound detected and H2DCF−DA is a non−fluorescent compound. MECs were incubated with H_2DCF−DA containing medium prior to each X−ray and measured the DCF fluorescence intensity by FACS which can differentiate the intracellular ROS concentration from the extracellular one.

In the APPJ treatment results, the DCF fluorescence intensity was increased by enhancement of the applied voltage to the APPJ and extension of treatment duration. As shown in figure 4.5, the DCF fluorescence intensity increased by less than twice by the voltage change from 5 kVp to 7 kVp. Two times of plasma exposure duration (condition 3 vs. condition 2) resulted in approximately two times of DCF fluorescence intensity. This result is in contrast with the change to more than thrice in DMPO−OH signal intensity (Figure 4.7).

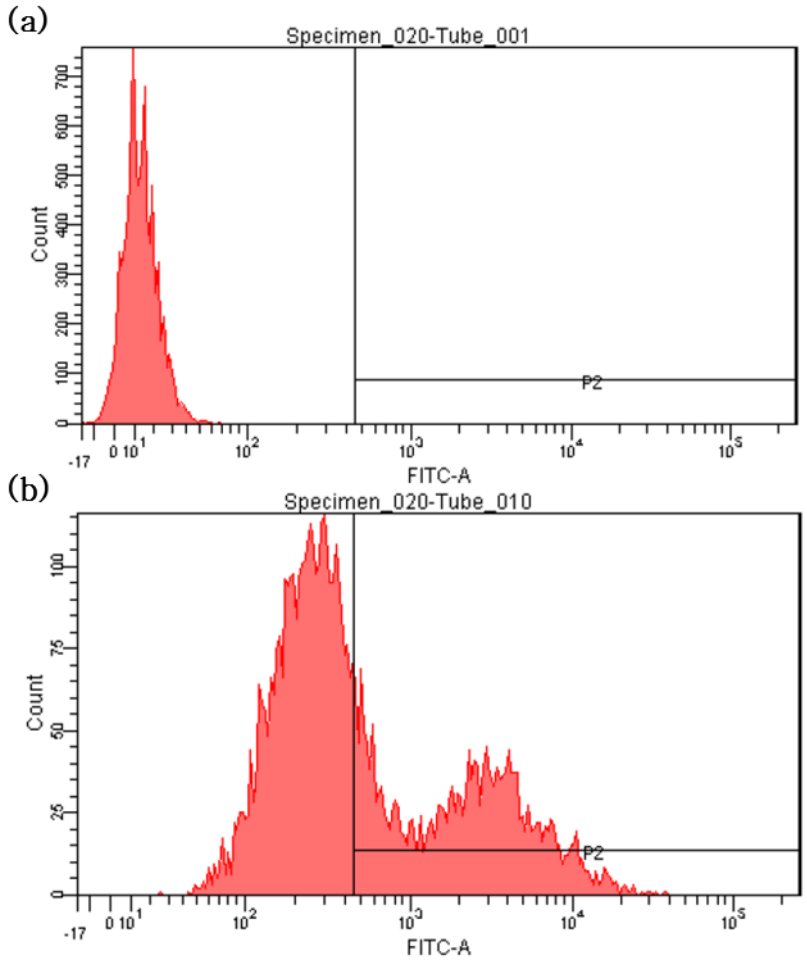

Figure 4.6 Results of DCF intensities measured in MECs after APPJ treatment. (a) DCF fluorescence intensity of non-treated cells (b) DCF fluorescence intensity of treated cells (7 kV, 2 SLM)

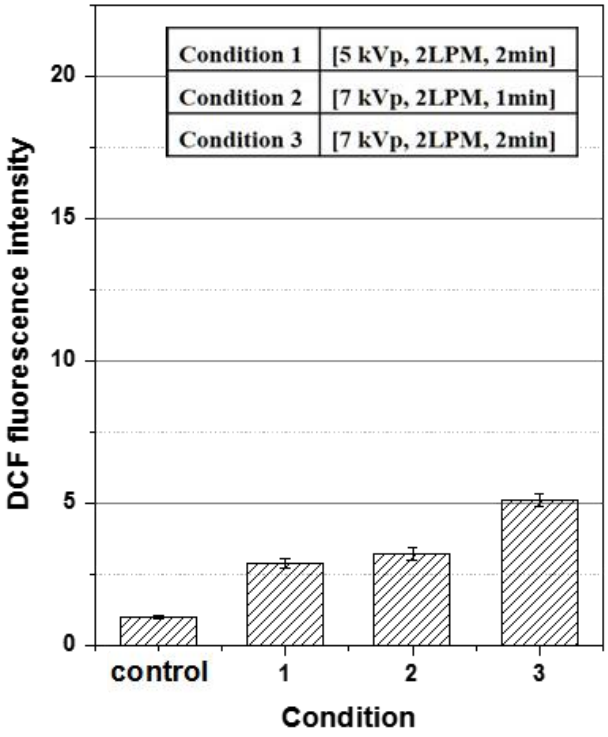

Figure 4.7 DCF fluorescence intensities under three operating conditions. Each data was normalized to the control. Each error bars indicates one standard error of the mean obtained from three independent experiments.

4.5 The clonogenic surviving fractions from X-ray irradiation and APPJ treatment

The clonogenic surviving fractions of MECs from X-ray exposure at doses of up to 10 Gy are presented in figure 4.8. The experimental data (solid squares) were fitted to a linear-quadratic curve (solid line): surviving fraction (SF) = $\exp[-0.223D-0.023D^2]$. The surviving fractions of cells from plasma treatments under conditions 1, 2, and 3 were marked (solid triangles) on the fitting curve. Radiation doses corresponding to those SF values under conditions 1, 2, and 3 were read at 4.5, 5.3, and 7.3 Gy, respectively.

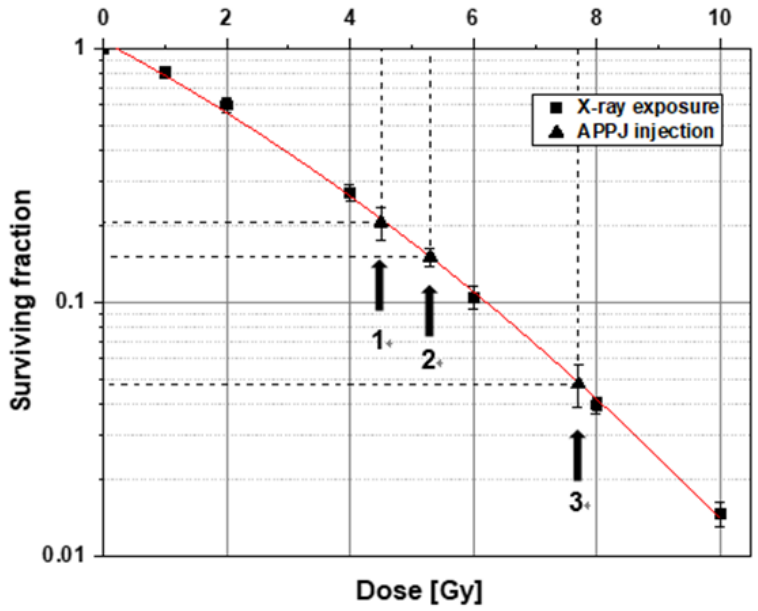

Figure 4.8 Surviving fractions of MECs from X-ray exposures of up to 10 Gy and plasma treatments under operational conditions 1, 2 and 3 of the APPJ device. The experimental data (solid squares) from radiation exposure were fitted to the solid curve. The solid triangles mark the clonogenic surviving fractions of MECs from plasma treatments under three different conditions 1, 2 and 3 of the APPJ device operation. Each error bar indicates one standard error of the mean obtained from three independent experiments.

4.6 Contribution of plasma-generated reactive species

Measurements of intracellular ROS were conducted after addition of each scavenger. APPJ treatment condition was fixed same as condition 2 in 4.4 (V_p: 7kV, 2 SLM, 1 min). As shown in figure 4.9, intracellular ROS concentration decreased to 96% of control with PTIO, and decreased to 33 % of control with catalase, and decreased to 58% with d-mannitol, respectively. It means scavenging H_2O_2 was most effective to inhibit intracellular ROS production. NO radical almost did not contribute for inducing production of intracellular ROS for plasma treatment.

Clonogenic assays were conducted after addition of each scavenger in medium. APPJ treatment condition was fixed same as condition 2 in 4.4 (V_p: 7kV, 2 SLM, 1 min). As shown in figure 4.10, SF increased to 135% compared to control with PTIO, increased to 175 % with catalase, and SF decreased to 93% with d-mannitol.

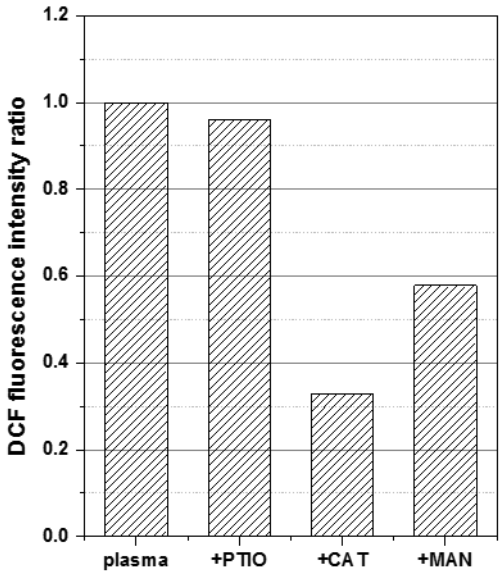

Figure 4.9 DCF fluorescence intensities with scavengers. Each PTIO (PTIO, 230 μM), Catalase (CAT, 60 U/ml), d-mannitol (MAN, 25 mM) was added in medium with MECs before plasma treatment. Plasma treatment condition was same as condition 2 in 4.4 (applied Vp: 7 kV, He gas flow: 2 SLM, treatment duration: 1 min). Each data was normalized to plasma treated control. (+PTIO: 0.96, +CAT: 0.33, +MAN: 0.58)

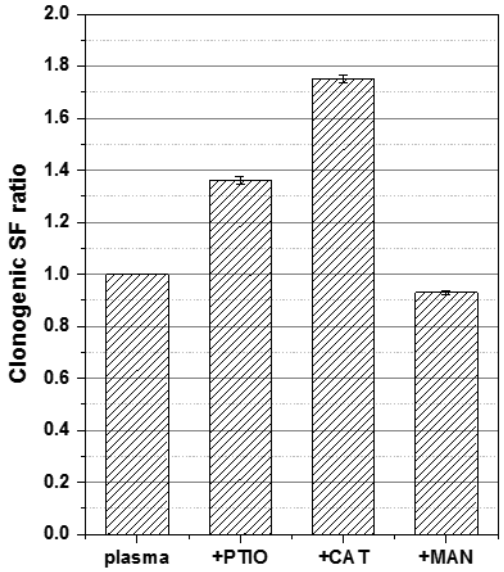

Figure 4.10 Clonogenic surviving fraction with scavengers. Each PTIO (PTIO, 230 μM), Catalase (CAT, 60 U/ml), d-mannitol (MAN, 25 mM) was added in medium with MECs before plasma treatment. Plasma treatment condition was same as condition 2 in 4.4 (applied Vp: 7 kV, He gas flow: 2 SLM, treatment duration: 1 min). Each data was normalized to plasma treated control. (+PTIO: 1.35, +CAT: 1.75, +MAN: 0.93)

* d-mannitol 에 의한 SF 이 감소한 결과가 보임.
* data set 수가 많지 않으며, 추후 실험 결과를 보완할 예정임.

CHAPTER 5

DISCUSSIONS

5.1 Analysis of OH radical production in medium

We measured DMPO-OH compound by ESR spectrometer, because OH radical itself was hard to detect directly due to very short lifetime as we referred in 3.3 [90-93]. It is known that the half-life of DMPO-OH is 14.5 min [96] and it was enough to detect by using ESR spectrometer.

DMPO-OH signal increased with X-ray dose, which showed the diminished efficiency of the unit dose at range of high dose [Figure 5.1]. The smaller value of signal intensity per dose at a higher dose may be attributed partly to the relatively short half-life of DMPO-OH as compared with the duration of experimental procedure. X-ray system delivered energy to the cells in vitro at a rate of 3.68 Gy/min and thus energy delivery upon exposures at 2 and 50 Gy took 1 and 13.6 min, respectively. An additional 6 min lapsed until ESR measurement after irradiation completion. Thus, approximately 7 min lapsed until ESR measurement after exposure to 2 Gy whereas approximately 19.6 min lapsed after exposure to 50 Gy. The total lapse from the start of DMPO-OH production by X-ray exposure until the ESR measurement increased with dose. The long lapse resulted in the dissociation of DMPO-OH product by a great portion. In consequence, the signal intensity per unit dose was low at a high dose.

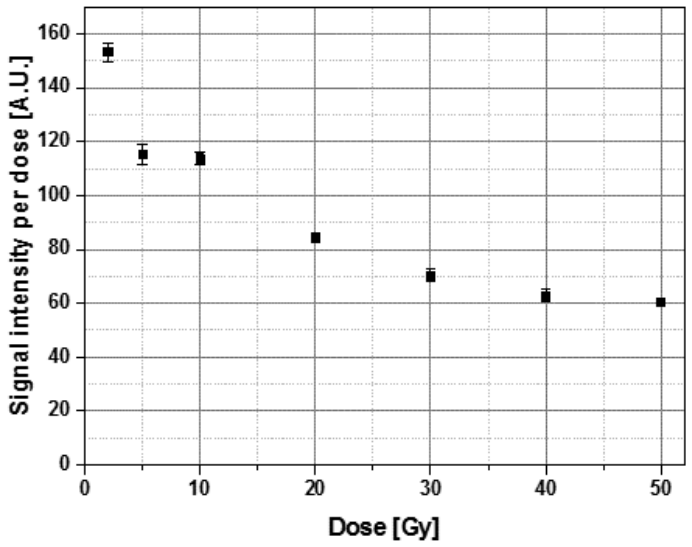

Figure 5.1 DMPO-OH signal intensities per unit dose in arbitrary unit measured at 6 min after 2-50 Gy of radiation irradiations. Each error bars indicates one standard error of the mean obtained from three independent experiments.

5.2 Analysis of OH radical production in APPJ treatment

The DMPO−OH signal production varies depending on the operating setup of the APPJ device and treatment duration [96]. In the experimental results, DMPO−OH signal intensity tends to increase proportionally to applied voltage of APPJ. Electron density linearly increases in plasma bullet with increased applied voltage [66] and thus, more OH radicals would be produced from electron dissociation. The OH radicals produced in plasma are flown into the culture medium with gas flow [67]. Consequently, the OH radical concentration in culture medium increases.

Plasma treatment lasted for 2, 3, and 4 min. Thus, the time lapse including plasma treatment until ESR measurement ranged from 8 min to 10 min, which was shorter than the half−life of the DMPO−OH signal. As a result, the DMPO−OH signal intensity was linearly proportional to the duration of plasma treatment. As shown in figure 4.2, the effect of voltage increase from 5 kVp to 7 kVp was offset by the effect of shortened (from 2 min to 1 min) treatment (condition 2 versus condition 1). The effect of voltage increase from 5 kVp to 7 kVp (condition 3 versus condition 1) was comparable with that of prolonged (from 1 min to 2 min) treatment (condition 3 versus condition 2).

5.3 Comparison of X-ray irradiation and APPJ treatment in ROS production

We compared the results of the ROS production between X-ray and APPJ quantitatively. First, the OH radical production in culture medium was quantitated by DMPO-OH signal intensity Next, the intracellular production of ROS radicals was quantitated by DCF fluorescence intensity. At every condition, we corresponded with the plasma-generated ROS concentration to equivalent radiation dose value in figure 5.2

The plasma treatment conditions of 1, 2, and 3 were equivalent in OH radical production in the culture medium to the X-ray doses of approximately 2.34, 2.27, and 5.39 Gy, respectively [Figure 5.2(a)]. Regarding intracellular ROS production, the equivalent X-ray doses to the plasma treatment conditions 1, 2, and 3 were 1.96, 2.32, and 3.42 Gy, respectively [Figure 5.2(b)]. Table 5.1 summarizes that the equivalent doses of conditions 1, 2, and 3 for the comparable DCF production (1.96, 2.32 and 3.42 Gy) are lower than for the comparable DMPO-OH production (2.34, 2.27 and 5.39 Gy), respectively. The low equivalent doses of plasma treatment for DCF production implies that plasma treatment is less efficient in intracellular ROS production as compared for OH production in the culture medium. Notably, intracellular ROS radical production is attributed to direct energy delivery of radiation to cellular molecules, whereas it is attributed to indirect plasma action via H_2O_2 production in the culture medium.

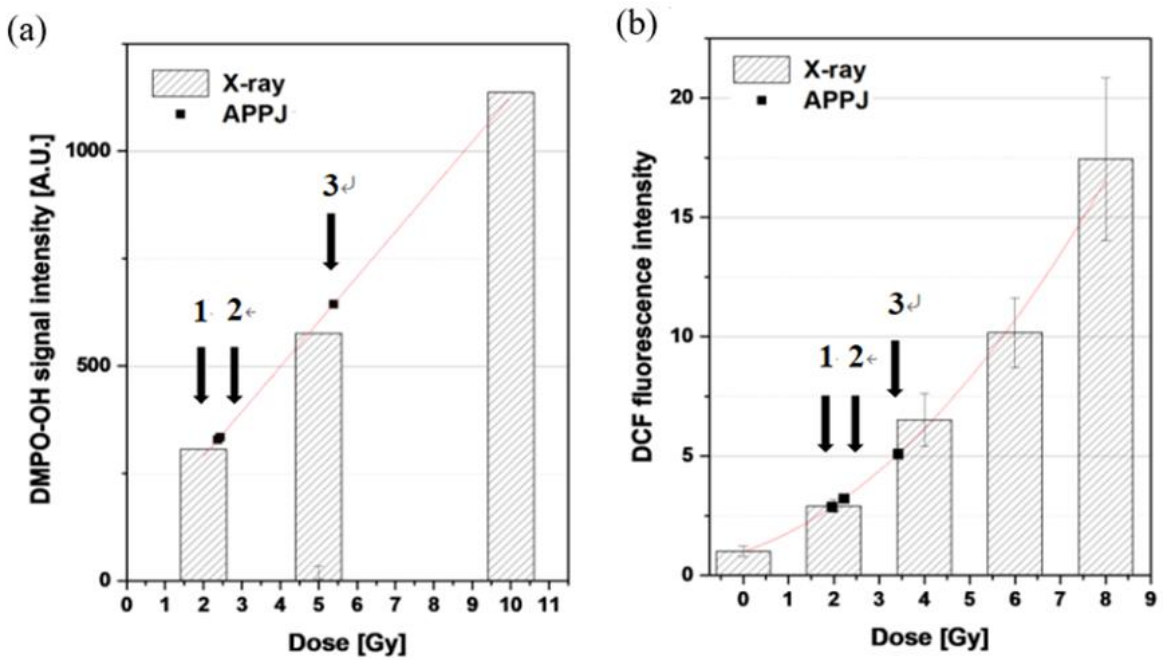

Figure 5.2 Effects of radiation exposure and plasma treatment in terms of (a) DMPO−OH signal intensity and (b) DCF fluorescence intensity. The DMPO−OH and DCF intensity data are fitted to a linear and a polynomial function, respectively. Arrows indicate the DMPO−OH and DCF intensities induced by plasma treatments under three operational setups (conditions 1, 2, and 3) of the APPJ device.

Table 5.1 DMPO-OH signal and DCF fluorescence intensities under three different parametric setups of APPJ device operation and the X-ray doses that would cause the comparable DMPO-OH and DCF signal intensities to plasma treatments.

Operational conditions* of APPJ device		DMPO-OH signal intensity (AU)	DCF fluorescence intensity (% of the control)	X-ray dose† for comparable DMPO-OH production	X-ray dose‡ for comparable DCF production
1	(5 kVp, 2 LPM, 2 min)	329 ± 66**	287 ± 15	2.37 Gy	1.96 Gy
2	(7 kVp, 2 LPM, 1 min)	335 ± 13※	321 ± 22	2.43 Gy	2.22 Gy
3	(7 kVp, 2 LPM, 2 min)	644 ± 43	509 ± 20	5.39 Gy	3.42 Gy

*(applied voltage, helium gas flow rate, duration of treatment)

** standard error

†X-ray dose derived as in Fig. 6(a)

‡ X-ray dose as in Fig. 6(b)

※ data obtained by extrapolation from the data in Fig. 3(b)

5.4 Analysis to contribution of plasma-generated species

Non-thermal plasma-generated species include ROS and also RNS. Most papers reported that ROS contributes to cell death dominantly while RNS contributes minor effect [15-17]. It was necessary to analyze which plasma species would be dominant in our experiment due to customized APPJ device.

Table 5.2 contains results which ROS played dominant role in this study. All data were normalized to plasma-treated control. H_2O_2 was estimated as major species to inducing intracellular ROS and cell death. Scavenging NO was ineffective for inducing intracellular. However, scavenging NO increased survival fraction little compared to H_2O_2, which means RNS should not be neglected at all for plasma medicine. It was estimated that d-mannitol induced more cell death from results of clonogenic assay, but the number of dataset was not enough to analyze. It needs further experiments for statistical significance.

We hypothesized that inducing OH radical from plasma would be essential to quantify plasma dose. From these results, we could secure the main point that non-thermal plasma dose can be quantified with low LET radiation.

Table 5.2 The effect of scavengers of RONS generated from plasma. PTIO: NO scavenger, catalase: H_2O_2 scavenger, d-mannitol: OH scavenger.

	None	+PTIO	+CAT	+MAN
Intracellular ROS Concentration ratio (%)	100	96	33	58
Colonogenic surviving fraction ratio (%)	100	135	175	93

5.5 Equivalent dose of X-ray exposure to plasma treatment in cellular effect

Figure 5.3 shows equivalent radiation doses which are corresponding to equivalent OH radical production in cell culture medium, intracellular ROS production or clonogenic cell death to our observations after plasma treatments. The equivalent X-ray dose means the level of X-ray exposure that would result in comparable amount of medium OH, or intracellular ROS production, or the comparable fraction of clonogenic cell death (=1-SF) to the plasma treatment. Considering that non-thermal plasma and X-rays have common point for inducing cell death by producing ROS (especially OH radical) [1,13,16,17], a high fraction of clonogenic cell death can be expected under the plasma condition that causes a great amount of ROS or OH production. Overall, our observations in figure 5.3 comply with the expectation, which condition 3 induced the highest equivalent X-ray dose in medium OH and intracellular ROS production and in the fraction of clonogenic cell death. Each of plasma treatment conditions 1, 2, and 3 corresponds to a higher value of equivalent X-ray dose in causing clonogenic cell death than in producing medium OH or intracellular ROS. This result means that plasma treatment was more efficient in causing clonogenic cell death per unit production of medium OH or intracellular ROS than X-ray exposure.

In plasma treatment under condition 2, the equivalent X-ray dose in DMPO-OH signal production (2.43 Gy) is comparable with that in DCF fluorescence generation (2.22 Gy). This finding means that plasma treatment under condition 2 produced DMPO-OH signal and DCF fluorescence at similar intensity ratios to the DMPO-OH signal and DCF fluorescence, respectively, induced by X-ray exposure. In plasma treatment under condition 3, the equivalent X-ray dose in DMPO-OH

signal production (5.39 Gy) is higher than that in DCF fluorescence generation (3.42 Gy). The loss of transportation from medium to inner cell would be main reason for the lower intracellular ROS production. The equivalent radiation dose in DMPO-OH signal production increased by over 120%, whereas that in DCF fluorescence generation increased by approximately 55% (see Table 5.1). Notably, the equivalent dose with regard to the fraction of clonogenic cell death increased by approximately 45% (5.3 Gy to 7.7 Gy) due to the increased duration of plasma treatment from 1 min to 2 min (Table 5.2). Clonogenic cell death is attributed presumably to the intracellular ROS production rather than to the medium OH production.

In plasma treatment condition 2 as compared with the condition 1, the voltage applied to the APPJ device was raised from 5 kVp to 7 kVp, whereas the treatment duration was reduced from 2 min to 1 min. The DMPO-OH signal (and thus its equivalent radiation dose) changed by less than 2%, whereas the DCF fluorescence intensity increased by approximately 13% (Table 5.1). Clonogenic cell death increased by approximately 7%. The loss in intracellular ROS production caused by reduced treatment duration was compensated by the great effectiveness of intracellular ROS production at a high voltage. The high voltage compensated the reduction of medium OH production caused by reduced treatment duration to a less extent. Overall, the net increase in intracellular ROS production resulted in the increased clonogenic cell death. A previous study informed that apoptotic cell death was switched to necrotic cell death with increased applied voltage [97].

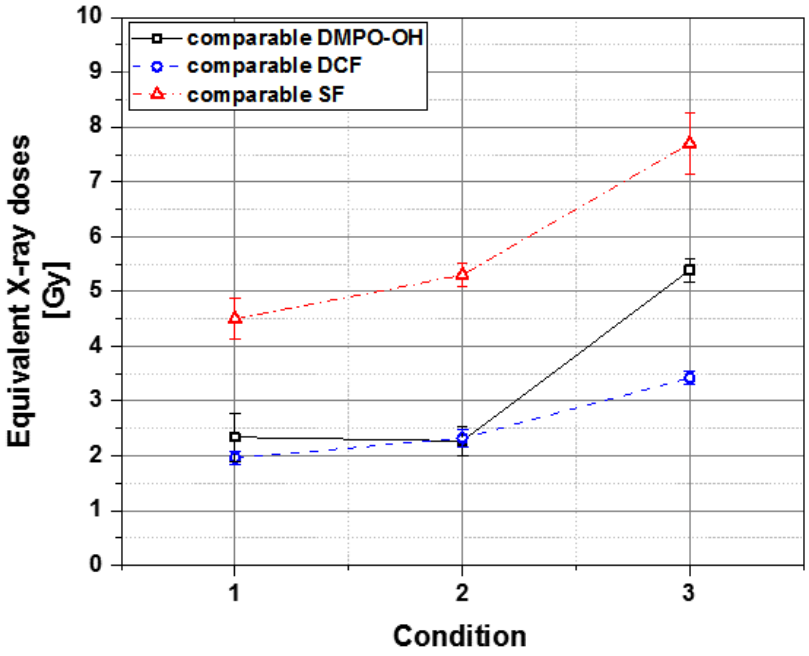

Figure 5.3. The equivalent X-ray doses in DCF fluorescence and DMPO-OH signal productions, and the fractional clonogenic cell death observed in MECs after plasma treatment under three (1, 2, and 3) operational conditions of APPJ device. Each data point was obtained from three to five independent experiments. Error bars indicate one standard errors for individual mean values.

Table 5.3 Surviving fractions of MECs from plasma treatments under three different operational conditions of the APPJ device and the approximate X-ray doses that would cause the comparable fractions of clonogenic cell death.

Operational conditions* of APPJ device		Clonogenic surviving fraction (SF)	Fraction of clonogenic cell death (1-SF)	X-ray dose for comparable fraction of clonogenic cell death (1-SF)
1	(5 kVp, 2 LPM, 2 min)	0.206 ± 0.029**	0.794	4.5 Gy
2	(7 kVp, 2 LPM, 1 min)	0.151 ± 0.013	0.849	5.3 Gy
3	(7 kVp, 2 LPM, 2 min)	0.048 ± 0.009	0.952	7.7 Gy

*(applied voltage, helium gas flow rate, duration of treatment)

**standard error

5.6 Consideration on the anti-cancer effect of non-thermal plasma

ROS are generated intrinsically in biological systems as metabolic byproducts in inflammation or produced by NADPH oxidase in the mitochondrial electron transport system etc [13]. At low concentration, ROS play as positive roles in tissue repair or cell proliferation, while at high concentration, ROS induce uncontrolled cell activity such as apoptosis, or mitochondrial dysfunction, and mutagenesis [13,98].

In the last years, several studies have pointed out the connection between ROS production and cancer treatments such as chemotherapeutics and ionizing radiation [99,100]. Most chemotherapeutic agents and ionizing radiation are used to directly kill cancer cells via generating ROS which can block cell cycle. However, Additional mutations in a cancer cell express increased levels of antioxidant proteins to protect from ROS, which cancer cell become easily resistant to radiation or chemotherapeutics. Because high level of intrinsic ROS concentration in cancer cell, it can result from increased modified oxidase activity.

While the conventional therapies have the disadvantage on anti-cancer treatment [101], non-thermal plasma which combining nitrogenous stress with oxidative stress might avoid such resistant. Several studies reported that RNS such as NO and other related compounds might have synergistic effect for inducing cancer cell death with ROS [13,23,80]. The equivalent concentration of H_2O_2 by use of chemical treatments in cellular medium induced less cell damage than plasma-treated experiments. RNS has minor effect for inducing cell death, however, can sensitize tumors to chemotherapy and radiation [101].

There are debates about combined treatment of plasma and radiation. Moniruzzaman et al. reported that combined treatment with radiation (5 Gy) and He-plasma (60s) showed only

additive enhancement apoptosis [71]. The author reported that radiation exposure did not increase any membrane fluidity, while hyperthermia treatment increased it. In contrary, Lin et al. reported plasma treatment enhanced radiation-induced DNA damage and inhibition of the tumor growth [102]. In this paper, plasma treatment prior to radiation sensitized radiation exposure to cell by inducing cell cycle arrest.

There is still much to be studied about the role of RNS in synergistic effect with ROS. It needs to study non-thermal plasma which generated various RONS at the same time for effective cancer treatment.

CHAPTER 6

CONCLUSION

Application of non-thermal plasma in medical area has been developing since 2000. Since plasma treatment was known to manipulate cell, a variety of application from microorganism deactivation, wound healing, coagulation, and to cancer treatment has been studying in many laboratories. Among them, selective anti-cancer effect of plasma medicine is one of the most important area.

Despite of popularity of plasma medicine, one of the main problem is the absence of the unity of plasma dosimetry. Because of this situation, many studies have been applied the operational parameters empirically to adjust plasma dose. And most laboratories are using own handicraft plasma discharge device, producing reproducibility is difficulty for leading commercialization of plasma medicine.

To solve this problem, we compared plasma with radiation dose which is well standardized in energy deposition to matter. Because both low LET radiation and non-thermal plasma have a common sense for producing free radical, we hypothesized that equivalent levels of radical production by radiation could assure quantification of plasma dose.

The principal conclusions of this study are:

1. We quantified medium OH and intracellular ROS productions which were considered as common indices for the bioeffects of radiation and plasma.

2. The equivalent X-ray dose to each operational setup of APPJ device was defined as the X-ray dose that would induce comparable radical production or the comparable fraction of clonogenic cell death to plasma treatment.

3. The operational setup of the APPJ device inducing a great radical (medium OH or intracellular ROS) production corresponded to the high fraction of clonogenic cell death. In plasma treatment, the clonogenic cell death was better predicted by intracellular ROS production rather than by medium OH production.

4. Considering that different cell lines showed different radiosensitivity to X-ray exposures, we presume that equivalent radiation doses of other cell lines to the same plasma treatment might be different. Nevertheless, the mechanism of inducing clonogenic cell death via intracellular ROS production would still apply to other cell lines.

We conducted simplification for assumption which radiation deposited energy in cells only indirect pathway and only OH radical was quantified for plasma treatment. However, comparison on main pathway of each treatment induces a good correspondence for inducing cell death. Selectivity of plasma on cancer cell death comes from a speculation that basal ROS concentration is higher than that of normal cells. To induce elevated ROS level in both cells adequately would be the essential for cancer treatment of plasma. This study suggests the equivalent radiation dose for quantifying plasma dose consistently.

REFERENCES

[1] Fridman, G., Friedman, G., Gutsol, A., Shekhter, A. B., Vasilets, V. N., & Fridman, A. (2008). Applied plasma medicine. Plasma processes and polymers, 5(6), 503-533.

[2] Shashurin, A., Keidar, M., Bronnikov, S., Jurjus, R. A., & Stepp, M. A. (2008). Living tissue under treatment of cold plasma atmospheric jet. Applied Physics Letters, 93(18), 181501.

[3] Heinlin, J., Morfill, G., Landthaler, M., Stolz, W., Isbary, G., Zimmermann, J. Shimizu, T. & Karrer, S. (2010). Plasma medicine: possible applications in dermatology. JDDG: Journal der Deutschen Dermatologischen Gesellschaft, 8(12), 968-976.

[4] Wu, H., Sun, P., Feng, H., Zhou, H., Wang, R., Liang, Y., Lu, J., Zhu, W., Zhang, J. & Fang, J. (2012). Reactive oxygen species in a non-thermal plasma microjet and water system: generation, conversion, and contributions to bacteria inactivation–an analysis by electron spin resonance spectroscopy. Plasma Processes and Polymers, 9(4), 417-424.

[5] Lee, H. W., Kim, G. J., Kim, J. M., Park, J. K., Lee, J. K., & Kim, G. C. (2009). Tooth bleaching with nonthermal atmospheric pressure plasma. Journal of endodontics, 35(4), 587-591.

[6] Farin, G., & Grund, K. E. (1994). Technology of argon plasma coagulation with particular regard to endoscopic applications. Endoscopic surgery and allied technologies, 2(1), 71-77.

[7] Grund, K. E., Storek, D., & Farin, G. (1994). Endoscopic argon plasma coagulation (APC) first clinical experiences in flexible endoscopy. Endoscopic surgery and allied technologies, 2(1), 42-46.

[8] Ginsberg, G. G., Barkun, A. N., Bosco, J. J., Burdick, J. S., Isenberg, G. A., Nakao, N., Petersen, B. T., Silverman, W. B., Slivka, A. & Kelsey, P. B. (2002). The argon plasma coagulator: February 2002. Gastrointestinal endoscopy, 55(7), 807-810.

[9] Laroussi, M. (2018). Plasma medicine: A brief introduction. Plasma, 1(1), 47-60.

[10] Laroussi, M., Lu, X., & Keidar, M. (2017). Perspective: The physics, diagnostics, and applications of atmospheric pressure low temperature plasma sources used in plasma medicine. Journal of Applied Physics, 122(2), 020901.

[11] Shekhter, A. B., Kabisov, R. K., Pekshev, A. V., Kozlov, N. P., & Perov, Y. L. (1998). Experimental and clinical validation of plasmadynamic therapy of wounds with nitric oxide. Bulletin of Experimental Biology and Medicine, 126(2), 829-834.

[12] Stoffels, E., Flikweert, A. J., Stoffels, W. W., & Kroesen, G. M. W. (2002). Plasma needle: a non-destructive atmospheric plasma source for fine surface treatment of (bio) materials. Plasma Sources Science and Technology, 11(4), 383.

[13] Keidar, M. (2015). Plasma for cancer treatment. Plasma Sources Science and Technology, 24(3), 033001.

[14] Yan, D., Sherman, J. H., & Keidar, M. (2017). Cold atmospheric plasma, a novel promising anti-cancer treatment modality. Oncotarget, 8(9), 15977.

[15] Veltmann, K. D., & von Voedtke, T. (2017). Plasma medicine-the current state of research and medical use. Plasma Phys. The control. Fusion, 59, 014031.

[16] Kim, Y. H., Hong, Y. J., Baik, K. Y., Kwon, G. C., Choi, J. J., Cho, G. S., Uhm, H. S. & Choi, E. H. (2014). Measurement of reactive hydroxyl radical species inside the biosolutions during non-thermal atmospheric pressure plasma jet bombardment onto the solution. Plasma Chemistry and

Plasma Processing, 34(3), 457-472.
[17] Lin, A., Truong, B., Patel, S., Kaushik, N., Choi, E. H., Fridman, G., Fridman, A. & Miller, V. (2017). Nanosecond-pulsed DBD plasma-generated reactive oxygen species trigger immunogenic cell death in A549 lung carcinoma cells through intracellular oxidative stress. International journal of molecular sciences, 18(5), 966.
[18] Ahn, H. J., Kim, K. I., Kim, G., Moon, E., Yang, S. S., & Lee, J. S. (2011). Atmospheric-pressure plasma jet induces apoptosis involving mitochondria via generation of free radicals. PloS one, 6(11).
[19] Azzariti, A., Iacobazzi, R. M., Di Fonte, R., Porcelli, L., Gristina, R., Favia, P., Fracassi, F., Trizio, I., Silvestris, N. & Tommasi, S. (2019). Plasma-activated medium triggers cell death and the presentation of immune activating danger signals in melanoma and pancreatic cancer cells. Scientific reports, 9(1), 1-13.
[20] Hirst, A. M., Simms, M. S., Mann, V. M., Maitland, N. J., O'connell, D., & Frame, F. M. (2015). Low-temperature plasma treatment induces DNA damage leading to necrotic cell death in primary prostate epithelial cells. British journal of cancer, 112(9), 1536-1545.
[21] Adachi, T., Tanaka, H., Nonomura, S., Hara, H., Kondo, S. I., & Hori, M. (2015). Plasma-activated medium induces A549 cell injury via a spiral apoptotic cascade involving the mitochondrial-nuclear network. Free Radical Biology and Medicine, 79, 28-44.
[22] Judée, F., Fongia, C., Ducommun, B., Yousfi, M., Lobjois, V., & Merbahi, N. (2016). Short and long time effects of low temperature Plasma Activated Media on 3D multicellular tumor spheroids. Scientific reports, 6, 21421.
[23] Yan, D., Cui, H., Zhu, W., Nourmohammadi, N., Milberg, J., Zhang, L. G., Sherman, J. H. & Keidar, M. (2017). The specific vulnerabilities of cancer cells to the cold

atmospheric plasma-stimulated solutions. Scientific reports, 7(1), 1-12.

[24] Lin A., Chernets N., Han J., Alicea Y., Dobrynin D., Fridman G., Freeman T. A., Fridman A., Miller V. (2015). Non-Equilibrium Dielectric Barrier Discharge Treatment of Mesenchymal Stem Cells: Charges and Reactive Oxygen Species Play the Major Role in Cell Death. Plasma Processes and Polymers, 12(10), 1117-1127.

[25] Ghimire, B., Sornsakdanuphap, J., Hong, Y. J., Uhm, H. S., Weltmann, K. D., & Choi, E. H. (2017). The effect of the gap distance between an atmospheric-pressure plasma jet nozzle and liquid surface on OH and N_2 species concentrations. Physics of Plasmas, 24(7), 073502.

[26] Pei, X., Lu, Y., Wu, S., Xiong, Q., & Lu, X. (2013). A study on the temporally and spatially resolved OH radical distribution of a room-temperature atmospheric-pressure plasma jet by laser-induced fluorescence imaging. Plasma Sources Science and Technology, 22(2), 025023.

[27] Ninomiya, K., Ishijima, T., Imamura, M., Yamahara, T., Enomoto, H., Takahashi, K., Tanaka, Y., Uesugi, Y. & Shimizu, N. (2013). Evaluation of extra-and intracellular OH radical generation, cancer cell injury, and apoptosis induced by a non-thermal atmospheric-pressure plasma jet. Journal of Physics D: Applied Physics, 46(42), 425401.

[28] Kanazawa, S., Furuki, T., Nakaji, T., Akamine, S., & Ichiki, R. (2012). Measurement of OH radicals in aqueous solution produced by atmospheric-pressure LF plasma jet. Int. J. Plasma Environ. Sci. Technol., 6(2), 166-171.

[29] Rudolph, R., Francke, K. P. & Miessner, H. OH radicals as oxidizing agent for the abatement of organic pollutants in gas flows by dielectric barrier discharges. Plasmas Polym. 8, 153-161 (2003).

[30] Barnard, S., Bouffler, S., & Rothkamm, K. (2013). The shape of the radiation dose response for DNA double-

strand break induction and repair. Genome integrity, 4(1), 1.

[31] Schöllnberger, H., Mitchel, R. E. J., Azzam, E. I., Crawford-Brown, D. J., & Hofmann, W. (2002). Explanation of protective effects of low doses of γ-radiation with a mechanistic radiobiological model. International journal of radiation biology, 78(12), 1159-1173.

[32] Sheikh, M. S., Antinore, M. J., Huang, Y., & Fornace, A. J. (1998). Ultraviolet-irradiation-induced apoptosis is mediated via ligand independent activation of tumor necrosis factor receptor 1. Oncogene, 17(20), 2555-2563.

[33] Cadet, J., Sage, E., & Douki, T. (2005). Ultraviolet radiation-mediated damage to cellular DNA. Mutation Research/Fundamental and Molecular Mechanisms of Mutagenesis, 571(1-2), 3-17.

[34] Yoon, S. Y., Kim, K. H., Seol, Y. J., Kim, S. J., Bae, B., Huh, S. R., & Kim, G. H. (2016). Effects of metastable species in helium and argon atmospheric pressure plasma jets (APPJs) on inactivation of periodontopathogenic bacteria. Journal of the Korean Physical Society, 68(10), 1176-1191.

[35] Graves, D. B. (2017). Mechanisms of plasma medicine: coupling plasma physics, biochemistry, and biology. IEEE Transactions on Radiation and Plasma Medical Sciences, 1(4), 281-292.

[36] Winter J., Tresp H., Hammer M.U., Iseni S., Kupsch S., Schmidt-Bleker, A., Wende K., Dünnbier M., Masur K. & Weltmann K.D. (2014). Tracking plasma generated H2O2 from gas into liquid phase and revealing its dominant impact on human skin cells. Journal of Physics D: Applied Physics, 47(28), 285401.

[37] Kurake N., Tanaka H., Ishikawa K., Kondo T., Sekine M., Nakamura K., Kajiyama H., Kikkawa F., Mizuno M. & Hori

M. (2016). Cell survival of glioblastoma grown in medium containing hydrogen peroxide and/or nitrite, or in plasma-activated medium. Archives of biochemistry and biophysics, 605, 102-108.

[38] Girard, P. M., Arbabian, A., Fleury, M., Bauville, G., Puech, V., Dutreix, M., & Sousa, J. S. (2016). Synergistic effect of H 2 O 2 and NO 2 in cell death induced by cold atmospheric He plasma. Scientific reports, 6, 29098.

[39] Winter J., Tresp H., Hammer M.U., Iseni S., Kupsch S., Schmidt-Bleker, A., Wende K., Dünnbier M., Masur K. & Weltmann K.D. (2014). Tracking plasma generated H2O2 from gas into liquid phase and revealing its dominant impact on human skin cells. Journal of Physics D: Applied Physics, 47(28), 285401.

[40] Reuter S., Tresp H., Wende K., Hammer M. U., Winter J., Masur K., Schmidt-Bleker A. & Weltmann K. D. (2012). From RONS to ROS: tailoring plasma jet treatment of skin cells. IEEE Transactions on Plasma Science, 40(11), 2986-2993.

[41] Wang, M., Holmes, B., Cheng, X., Zhu, W., Keidar, M., & Zhang, L. G. (2013). Cold atmospheric plasma for selectively ablating metastatic breast cancer cells. PloS one, 8(9).

[42] Thiyagarajan, M., Anderson, H., & Gonzales, X. F. (2014). Induction of apoptosis in human myeloid leukemia cells by remote exposure of resistive barrier cold plasma. Biotechnology and bioengineering, 111(3), 565-574.

[43] Bruggeman, P., & Schram, D. C. (2010). On OH production in water containing atmospheric pressure plasmas. Plasma Sources Science and Technology, 19(4).

[44] Yoon, S. Y. (2015). Generation mechanism of hydroxyl radical in electrolyte streamer discharge (Doctoral dissertation), Preprint at http://hdl.handle.net/10371/118176

[45] Schram, D. C. (2008). Is plasma unique? The presence of electrons and the importance of charge. Plasma Sources Science and Technology, 18(1), 014003.
[46] Manion, J. A. (2008). NIST Chemical Kinetics Database, NIST Standard Reference Database 17, Version 7.0 (Web Version), Release 1.4. 3, Data version 2008.12. http://kinetics. nist. gov/
[47] Itikawa, Y., & Mason, N. (2005). Cross sections for electron collisions with water molecules. Journal of Physical and Chemical reference data, 34(1), 1-22.
[48] Itikawa, Y., & Mason, N. (2005). Cross sections for electron collisions with water molecules. Journal of Physical and Chemical reference data, 34(1), 1-22.
[49] Millar, T. J., Farquhar, P. R. A., & Willacy, K. (1997). The UMIST database for astrochemistry 1995. Astronomy and Astrophysics Supplement Series, 121(1), 139-185.
[50] Gordillo-Vázquez, F. J. (2008). Air plasma kinetics under the influence of sprites. Journal of Physics D: Applied Physics, 41(23), 234016.
[51] Kushner, M. J. (1999). Strategies for rapidly developing plasma chemistry models. Bull. Am. Phys. Soc, 44, 63.
[52] Herron, J. T., & Green, D. S. (2001). Chemical kinetics database and predictive schemes for nonthermal humid air plasma chemistry. Part II. Neutral species reactions. Plasma Chemistry and Plasma Processing, 21(3), 459-481.
[53] Baulch, D. L., Cobos, C. J., Cox, R. A., Frank, P., Hayman, G., Just, T., Kerr, J. A., Murrells, T., Pilling, M. J. & Walker, R. W. (1994). Summary table of evaluated kinetic data for combustion modeling: Supplement 1. Combustion and flame, 98(1-2), 59-79.
[54] Fridman, A. (2008). Plasma chemistry. Cambridge university press.
[55] NIST Chemistry Web Book, http://webbook.nist.gov/

chemistry.
[56] Liu, X. Y., Pei, X. K., Ostrikov, K., Lu, X. P., & Liu, D. W. (2014). The production mechanisms of OH radicals in a pulsed direct current plasma jet. Physics of Plasmas, 21(9), 093513.
[57] Karakas, E., Koklu, M., & Laroussi, M. (2010). Correlation between helium mole fraction and plasma bullet propagation in low temperature plasma jets. Journal of Physics D: Applied Physics, 43(15), 155202.
[58] Yue, Y., Wu, F., Cheng, H., Xian, Y., Liu, D., Lu, X., & Pei, X. (2017). A donut-shape distribution of OH radicals in atmospheric pressure plasma jets. Journal of Applied Physics, 121(3), 033302.
[59] Yoon, S. Y., Kim, G. H., Kim, S. J., Bae, B., Kim, N. K., Lee, H., Bae, N., Ryu, S., Yoo, S. J. & Kim, S. B. (2017). Bullet-to-streamer transition on the liquid surface of a plasma jet in atmospheric pressure. Physics of Plasmas, 24(1), 013513.
[60] Lu, X., Naidis, G. V., Laroussi, M., Reuter, S., Graves, D. B., & Ostrikov, K. (2016). Reactive species in non-equilibrium atmospheric-pressure plasmas: Generation, transport, and biological effects. Physics Reports, 630, 1-84.
[61] Hu, J. T., Wang, J. G., Liu, X. Y., Liu, D. W., Lu, X. P., Shi, J. J., & Ostrikov, K. (2013). Effect of a floating electrode on a plasma jet. Physics of Plasmas, 20(8), 083516.
[62] Liu, D. X., Bruggeman, P., Iza, F., Rong, M. Z., & Kong, M. G. (2010). Global model of low-temperature atmospheric-pressure He^+ H_2O plasmas. Plasma Sources Science and Technology, 19(2), 025018.
[63] Sicard-Roselli C., Brun E., Gilles M., Baldacchino G., Kelsey C., McQuaid H., Polin C., Wardlow N. & Currell F. (2014). A new mechanism for hydroxyl radical production in irradiated nanoparticle solutions. small, 10(16), 3338-

3346.

[64] Fulford, J., Nikjoo, H., Goodhead, D. T., & O'Neill, P. (2001). Yields of SSB and DSB induced in DNA by Al K ultrasoft X-rays and α-particles: comparison of experimental and simulated yields. International journal of radiation biology, 77(10), 1053-1066.

[65] Joseph, P., Bhat, N. N., Copplestone, D., & Narayana, Y. (2014). Production of gamma induced reactive oxygen species and damage of DNA molecule in HaCaT cells under euoxic and hypoxic condition. Journal of Radioanalytical and Nuclear Chemistry, 302(2), 983-988.

[66] Shrestha, R., Tyata, R. B., & Subedi, D. P. (2013). Effect of applied voltage in electron density of homogeneous dielectric barrier discharge at atmospherice pressure. Himalayan Physics, 4, 10-13.

[67] Pei, X., Wu, S., Xian, Y., Lu, X., & Pan, Y. (2014). On OH density of an atmospheric pressure plasma jet by laser-induced fluorescence. IEEE Transactions on Plasma Science, 42(5), 1206-1210.

[68] Uhm, H. S. (2015). Generation of various radicals in nitrogen plasma and their behavior in media. Physics of Plasmas, 22(12), 123506.

[69] Ahn, H. J., Kim, K. I., Hoan, N. N., Kim, C. H., Moon, E., Choi, K. S., Yang, S. S. & Lee, J. S. (2014). Targeting cancer cells with reactive oxygen and nitrogen species generated by atmospheric-pressure air plasma. PloS one, 9(1).

[70] Hong, S. H., Szili, E. J., Jenkins, A. T. A., & Short, R. D. (2014). Ionized gas (plasma) delivery of reactive oxygen species (ROS) into artificial cells. Journal of Physics D: Applied Physics, 47(36), 362001.

[71] Moniruzzaman, R., Rehman, M. U., Zhao, Q. L., Jawaid, P., Takeda, K., Ishikawa, K., Hori, M., Tomihara, K., Noguchi, K. & Noguchi, M. (2017). Cold atmospheric helium plasma

causes synergistic enhancement in cell death with hyperthermia and an additive enhancement with radiation. Scientific reports, 7(1), 1-12.

[72] Bienert, G. P., Schjoerring, J. K., & Jahn, T. P. (2006). Membrane transport of hydrogen peroxide. Biochimica et Biophysica Acta (BBA)-Biomembranes, 1758(8), 994-1003.

[73] Bienert, G. P., & Chaumont, F. (2014). Aquaporin-facilitated transmembrane diffusion of hydrogen peroxide. Biochimica et Biophysica Acta (BBA)-General Subjects, 1840(5), 1596-1604.

[74] Almasalmeh, A., Krenc, D., Wu, B., & Beitz, E. (2014). Structural determinants of the hydrogen peroxide permeability of aquaporins. The FEBS journal, 281(3), 647-656.

[75] Ishibashi, K., Hara, S., & Kondo, S. (2009). Aquaporin water channels in mammals. Clinical and experimental nephrology, 13(2), 107-117.

[76] Yan, D., Xiao, H., Zhu, W., Nourmohammadi, N., Zhang, L. G., Bian, K., & Keidar, M. (2017). The role of aquaporins in the anti-glioblastoma capacity of the cold plasma-stimulated medium. Journal of Physics D: Applied Physics, 50(5), 055401.

[77] Takahashi, M. A., & Asada, K. (1983). Superoxide anion permeability of phospholipid membranes and chloroplast thylakoids. Archives of Biochemistry and Biophysics, 226(2), 558-566.

[78] Bekeschus, S., Kolata, J., Winterbourn, C., Kramer, A., Turner, R., Weltmann, K. D., Bröker, B. & Masur, K. (2014). Hydrogen peroxide: A central player in physical plasma-induced oxidative stress in human blood cells. Free radical research, 48(5), 542-549.

[79] Xu, D., Liu, D., Wang, B., Chen, C., Chen, Z., Li, D., Yang, Y., Chen, H. & Kong, M. G. (2015). In situ OH generation

from O2- and H2O2 plays a critical role in plasma-induced cell death. PloS one, 10(6).

[80] Yan, D., Talbot, A., Nourmohammadi, N., Cheng, X., Canady, J., Sherman, J., & Keidar, M. (2015). Principles of using cold atmospheric plasma stimulated media for cancer treatment. Scientific reports, 5, 18339.

[81] Balzer, J., Heuer, K., Demir, E., Hoffmanns, M. A., Baldus, S., Fuchs, P. C., Awakowicz, P., Suschek, C. V. & Opländer, C. (2015). Non-thermal dielectric barrier discharge (DBD) effects on proliferation and differentiation of human fibroblasts are primary mediated by hydrogen peroxide. PLoS One, 10(12).

[82] Winter, J., Wende, K., Masur, K., Iseni, S., Dünnbier, M., Hammer, M. U., Tresp, H., Weltmann, K. D. & Reuter, S. (2013). Feed gas humidity: a vital parameter affecting a cold atmospheric-pressure plasma jet and plasma-treated human skin cells. Journal of Physics D: Applied Physics, 46(29), 295401.

[83] Riley, P. A. (1994). Free radicals in biology: oxidative stress and the effects of ionizing radiation. International journal of radiation biology, 65(1), 27-33.

[84] Alpen, E. L. (1997). Radiation biophysics. Academic press.

[85] Eaton, G. R., Eaton, S. S., Barr, D. P., & Weber, R. T. (2010). Quantitative Epr. Springer Science & Business Media.

[86] Huie, R. E. (2003). NDRL/NIST Solution Kinetics Database on the WEB. Journal of Research (NIST JRES)-, 108(Journal of Research (NIST JRES)).

[87] Attri, P., Kim, Y. H., Park, D. H., Park, J. H., Hong, Y. J., Uhm, H. S., Kim, K. N., Fridman, A. & Choi, E. H. (2015). Generation mechanism of hydroxyl radical species and its lifetime prediction during the plasma-initiated ultraviolet (UV) photolysis. Scientific reports, 5, 9332.

[88] Girard, F., Badets, V., Blanc, S., Gazeli, K., Marlin, L.,

Authier, L., Svarnas, P., Sojic, N., Clément, F. & Arbault, S. (2016). Formation of reactive nitrogen species including peroxynitrite in physiological buffer exposed to cold atmospheric plasma. Rsc Advances, 6(82), 78457−78467.

[89] Verreycken, T., Van der Horst, R. M., Baede, A. H. F. M., Van Veldhuizen, E. M., & Bruggeman, P. J. (2012). Time and spatially resolved LIF of OH in a plasma filament in atmospheric pressure He-H2O. Journal of Physics D: Applied Physics, 45(4), 045205.

[90] Murphy, D. M. (2009). EPR (Electron Paramagnetic Resonance) spectroscopy of polycrystalline oxide systems.

[91] Anzai, K., Aikawa, T., Furukawa, Y., Matsushima, Y., Urano, S., & Ozawa, T. (2003). ESR measurement of rapid penetration of DMPO and DEPMPO spin traps through lipid bilayer membranes. Archives of biochemistry and biophysics, 415(2), 251−256.

[92] Madden, K. P., & Taniguchi, H. (2001). The role of the DMPO−hydrated electron spin adduct in DMPO−OH spin trapping. Free Radical Biology and Medicine, 30(12), 1374−1380.

[93] Bačić, G., Spasojević, I., Šećerov, B., & Mojović, M. (2008). Spin−trapping of oxygen free radicals in chemical and biological systems: New traps, radicals and possibilities. Spectrochimica Acta Part A: Molecular and Biomolecular Spectroscopy, 69(5), 1354−1366.

[94] Nishizawa, C., Takeshita, K., Ueda, J. I., Mizuno, M., Suzuki, K. T., & Ozawa, T. (2004). Hydroxyl radical generation caused by the reaction of singlet oxygen with a spin trap, DMPO, increases significantly in the presence of biological reductants. Free radical research, 38(4), 385−392.

[95] Lee, J. H. (2013). Study on the Cytotoxic Equivalency of Plasma and Radiation by Quantitating OH Radical Production (Doctoral dissertation), Preprint at

http://hdl.handle.net/10371/123459
Yoon, S. Y. (2015). Generation mechanism of hydroxyl radical in electrolyte streamer discharge (Master' s dissertation), Preprint at http://hdl.handle.net/10371/118176
[96] Thirumdas, R., Kothakota, A., Annapure, U., Siliveru, K., Blundell, R., Gatt, R., & Valdramidis, V. P. (2018). Plasma activated water (PAW): chemistry, physico-chemical properties, applications in food and agriculture. Trends in food science & technology, 77, 21-31.
[97] Kim, S. J., & Chung, T. H. (2016). Cold atmospheric plasma jet-generated RONS and their selective effects on normal and carcinoma cells. Scientific reports, 6, 20332.
[98] Trachootham, D., Alexandre, J., & Huang, P. (2009). Targeting cancer cells by ROS-mediated mechanisms: a radical therapeutic approach?. Nature reviews Drug discovery, 8(7), 579-591.
[99] Jha, N., Ryu, J. J., Choi, E. H., & Kaushik, N. K. (2017). Generation and role of reactive oxygen and nitrogen species induced by plasma, lasers, chemical agents, and other systems in dentistry. Oxidative medicine and cellular longevity, 2017.
[100] Liou, G. Y., & Storz, P. (2010). Reactive oxygen species in cancer. Free radical research, 44(5), 479-496.
[101] Graves, D. B. (2014). Reactive species from cold atmospheric plasma: implications for cancer therapy. Plasma Processes and Polymers, 11(12), 1120-1127.
[102] Lin, L., Wang, L., Liu, Y., Xu, C., Tu, Y., & Zhou, J. (2018). Non-thermal plasma inhibits tumor growth and proliferation and enhances the sensitivity to radiation in vitro and in vivo. Oncology reports, 40(6), 3405-3415.

국 문 초 록

최근 저온 플라즈마를 활용하여 살균, 조직 회복, 암 치료 등의 목적으로 의학 분야에 대한 연구가 진행되고 있지만, 플라즈마의 선량 측정에 대한 개념이 확립되지 않아 연구의 진행에 어려움이 있다. 대부분 연구실에서는 자체 제작된 플라즈마 발생 장치를 운용하고 있는데, 연구자의 경험에 근거하여 플라즈마 처치 시간의 조절을 통해 선량을 조절하고 있다. 따라서, 본 연구는 등가방사선량의 개념을 활용하여 플라즈마 처치 정량화를 수행하였다.

저온 플라즈마는 전자기장, 열, 자외선 등의 물리적 인자와 활성산소종 및 반응성 질소종 등의 화학적 인자를 생성한다. 대부분의 연구는 반응성 산소, 그 중에서도 수산화기에 의한 역할이 중요한 것을 언급하고 있다. 저선질 방사선에 의한 세포 영향은 주로 방사성 물분해에 의해 생성된 수산화기에 의한 간접 작용에 의함이 알려져 있다. 플라즈마와 저선질 방사선 모두 주로 수산화기의 생성을 매개로 하여, 세포에 영향을 주는 사실을 고려할 때, 등가방사선에 의한 수산화기의 생성량 비교를 통해 플라즈마 처치에 대한 정량화가 가능하였다. 본 연구에서는 저온 플라즈마 발생을 위해서 APPJ 장치를, 저선질 방사선을 발생하기 위한 X-선 발생장치를 활용하였다. 수산화기의 경우 반감기가 수 μs 정도로 반응성이 크기 때문에, spin trap 물질인 DMPO를 이용하여 반감기를 870 s로 늘린 후, 전자스핀공명분석기를 사용하여 그 생성량을 측정하였다.

공통된 매개체를 생성하지만, 수산화기의 생성 방식에 대해서는 두 방식의 차이점이 존재한다. 저선질 방사선의 경우 투과력이 강해 세포의 내·외부에 균질하게 수산화기를 생성한다고 볼 수 있지만, 플라즈마는 투과력이 없어 수산화기의 생성은 주로 세포 외부에

생성된다고 볼 수 있다. 따라서, 본 실험에서는 in vitro 상에서 세포를 포함하고 있는 배양액에서 실험을 진행하였기 때문에 DCFH 물질을 이용하여 세포 내부에 생성된 수산화기의 농도를 정량적으로 측정하였다. 플라즈마 또는 방사선에 의한 세포 독성 확인을 위해 세포 군집형성능 실험을 진행하였다.

플라즈마에 의해 생성된 세포 배양액 내의 수산화기 농도, 세포 내부에 생성된 수산화기의 농도, 그리고 군집형성능과 동등한 수산화기 생성량 또는 군집형성능을 보이는 등가방사선량을 도출하고 분석하였다. 그 결과로써 세포 내부의 수산화기 농도에 상응하는 등가방사선량과 세포 군집형성능에 상응하는 등가방사선량에 대한 상호 연관성에 대한 결론을 이끌어낼 수 있었다. 플라즈마에 의한 세포 독성은 세포 내부에 생성된 수산화기에 강한 연관성을 띄고 있으며, 이에 대한 등가방사선량을 활용한다면 다양한 연구에서 활용되는 플라즈마 처치에 대한 정량화가 가능해질 수 있다고 예상한다.

주요어 : 플라즈마 의학, 저온 플라즈마, 정량화, 등가방사선량
학 번 : 2013-23185